BRL MR 3810

DTIC FILE COPY

(2)

MEMORANDUM REPORT BRL-MR-3810

BRL

AD-A219 106

THE AERODYNAMIC CHARACTERISTICS OF .50 BALL, M33, API, M8, AND APIT, M20 AMMUNITION

ROBERT L. McCOY

JANUARY 1990

U.S. ARMY LABORATORY COMMAND

BALLISTIC RESEARCH LABORATORY
ABERDEEN PROVING GROUND, MARYLAND

90 03 15 029

UNCLASSIFIED
SECURITY CLASSIFICATION OF THIS PAGE

REPORT DOCUMENTATION PAGE

Form Approved
OMB No. 0704-0188

1a. REPORT SECURITY CLASSIFICATION: UNCLASSIFIED

1b. RESTRICTIVE MARKINGS:

2a. SECURITY CLASSIFICATION AUTHORITY:

2b. DECLASSIFICATION / DOWNGRADING SCHEDULE:

3. DISTRIBUTION / AVAILABILITY OF REPORT: Approved for public release; distribution is unlimited

4. PERFORMING ORGANIZATION REPORT NUMBER(S): BRL-MR-3810

5. MONITORING ORGANIZATION REPORT NUMBER(S):

6a. NAME OF PERFORMING ORGANIZATION: USA Ballistic Research Laboratory

6b. OFFICE SYMBOL (If applicable): SLCBR-LF-T

6c. ADDRESS (City, State, and ZIP Code): Aberdeen Proving Ground, MD 21005-5066

7a. NAME OF MONITORING ORGANIZATION:

7b. ADDRESS (City, State, and ZIP Code):

8a. NAME OF FUNDING / SPONSORING ORGANIZATION: USARDEC Fire Control

8b. OFFICE SYMBOL (If applicable): SMCAR-FSF-BD

8c. ADDRESS (City, State, and ZIP Code): Picatinny Arsenal, NJ 07806-5000

9. PROCUREMENT INSTRUMENT IDENTIFICATION NUMBER:

10. SOURCE OF FUNDING NUMBERS

PROGRAM ELEMENT NO	PROJECT NO	TASK NO	WORK UNIT ACCESSION NO
62618A	1L1 62618AH80		

11. TITLE (Include Security Classification): The Aerodynamic Characteristics of Caliber .50 Ball, M33, API, M8, and APIT, M20 Ammunition

12. PERSONAL AUTHOR(S): McCOY, Robert L.

13a. TYPE OF REPORT: MEMORANDUM

13b. TIME COVERED: FROM ______ TO ______

14. DATE OF REPORT (Year, Month, Day): 1989 December 5

15. PAGE COUNT: 75

16. SUPPLEMENTARY NOTATION:

17. COSATI CODES

FIELD	GROUP	SUB-GROUP
19	01	

18. SUBJECT TERMS (Continue on reverse if necessary and identify by block number):
Caliber .50 Bullets; Aerodynamic Characteristics; Aerodynamic Drag; Gyroscopic Stability; Dynamic Stability; Yaw Limit-Cycle

19. ABSTRACT (Continue on reverse if necessary and identify by block number)

The caliber .50 Ball, M33, API, M8 and APIT, M20 munitions were recently fired in the BRL spark photography ranges, to determine the complete aeroballistic characteristics required for a fire control study. Aerodynamic drag, gyroscopic stability, dynamic stability and yaw damping rates were determined at supersonic, transonic and subsonic speeds. The observed non-linear behavior of the Magnus moment coefficient predicts a slow arm limit cycle yaw at transonic and subsonic speeds.

20. DISTRIBUTION / AVAILABILITY OF ABSTRACT: ☐ UNCLASSIFIED/UNLIMITED ☒ SAME AS RPT ☐ DTIC USERS

21. ABSTRACT SECURITY CLASSIFICATION: UNCLASSIFIED

22a. NAME OF RESPONSIBLE INDIVIDUAL: Robert L. McCoy

22b. TELEPHONE (Include Area Code): 301-278-3880

22c. OFFICE SYMBOL: SLCBR-LF-T

DD Form 1473, JUN 86 — Previous editions are obsolete.

SECURITY CLASSIFICATION OF THIS PAGE
UNCLASSIFIED

INTENTIONALLY LEFT BLANK.

Table of Contents

INTENTIONALLY LEFT BLANK.

List of Figures

List of Figures (Continued)

List of Tables

Intentionally left blank.

I. Introduction

The caliber .50 Armor Piercing Incendiary (API, M8) and Armor Piercing Incendiary Tracer (APIT, M20) munitions were developed in 1943-44, for wartime service use in various versions of the caliber .50, M2, Browning Machine Gun. Reference 1 contains a summary of the limited aerodynamic data obtained during development testing of the new munitions. The drag coefficient was determined from resistance firings over solenoid velocity screens, and the stability was measured using yaw card techniques.

The caliber .50 Ball, M33 round was developed in 1961, as a companion ball munition to the API, M8, and was intended to be a ballistic match of the M8. Apparently, no aerodynamic tests were ever conducted for the M33 projectile. Some unpublished aerodynamic data for the APIT, M20 were obtained by M. J. Piddington in 1979, in support of the M1 Abrams tank development program. Piddington's spark photography range data are included in this report.

In November 1987, the Fire Control division of the U.S. Army Armament Research, Development and Engineering Center (ARDEC) requested that the Ballistic Research Laboratory (BRL) provide trajectory data for a fire control study involving current 7.62mm and caliber .50 infantry weapons. The BRL advised ARDEC that the existing aeroballistic data base for the caliber .50 munitions was insufficient to permit accurate trajectory predictions, and recommended that testing be conducted in the BRL spark photography ranges.[2,3] In early April 1988, test material and funding for the BRL spark range firings of caliber .50 munitions were received from ARDEC.

Final plans for the spark photography range tests were nearing completion when the Air Force Armament Laboratory at Eglin Air Force Base, Florida, requested that the BRL conduct large-yaw firings of the caliber .50, API, M8 projectile in the Free Flight Aerodynamics Range [2] to provide aeroballistic data for side-fire from high speed aircraft. By mutual agreement between the BRL, ARDEC, and the Air Force, the two aeroballistic tests were combined, and the Air Force supplied additional funding to the BRL for the large-yaw firings. This report presents all the modern aeroballistic data collected in the two BRL spark photography ranges, for the caliber .50 Ball, M33, API, M8 and APIT, M20 munitions.

II. Test Procedure and Material

Figure 1 is a photograph of the three caliber .50 projectiles. Figure 2 is a photograph of the BRL Aerodynamics Range (circa 1958), and Figure 3 illustrates the local and master coordinate systems for the range.

Physical measurements were taken on a sample of five projectiles of each type. The average physical properties of the test projectiles are listed in Table 1. The Ball, M33, API, M8, and APIT, M20 designs all have the same nominal external dimensions, and differ only in minor surface details, such as rolled versus machined cannelures. Figure 4 is a sketch of the exterior contour, common to all three projectiles.

All test rounds were fired from a 114.3 cm (45 inch) caliber .50 Mann barrel, with a uniform rifling twist rate of one turn in 38.1 cm (15 inches). Suitable propellants and charges were selected to achieve test velocities varying from 915 metres/second down to 240 metres/second. For the large-yaw firings of the API, M8, a half-muzzle type yaw inducer was used, with a lip length ranging from 6.35mm (1/4 inch) to 12.7mm (1/2 inch). Average yaw levels exceeding 12 degrees were obtained for several test rounds with the 12.7mm lip yaw inducer.

Live tracer firings of small caliber projectiles present a problem for the BRL Aerodynamics Range, because the light emitted from the tracer tends to fog the film. The APIT, M20 live tracer firings were conducted in the BRL Transonic Range, [3] with the gun backed off approximately 100 metres from the range entrance, to insure a fully burning tracer over the instrumentation. Transonic Range shadowgraphs of typical small caliber projectiles do not permit accurate measurement of yawing or swerving motion, so only drag is obtained from the live tracer firings.

Tracer-off firings of the APIT, M20 in the BRL Aerodynamics Range were conducted by pulling the projectiles, burning out the tracer mix, then firing the burned-out tracer round. All the Ball, M33 and API, M8 test firings were conducted in the Aerodynamics Range.

An interesting and useful by-product of spark photography range testing is the high quality flowfield visualization provided by the spark shadowgraphs. Figures 5 through 18 show the flowfields around the three caliber .50 bullets at various supersonic, transonic, and subsonic speeds. Most of the shadowgraphs were selected from range stations where the angle of attack was less than one degree; Figure 7 illustrates the effect of large angle of attack on the flow past the API, M8 projectile.

The round-by-round aerodynamic data obtained for the three caliber .50 bullets are listed in Tables 2, 3 and 4. Free flight motion parameters for the three bullets are listed in Tables 5, 6 and 7. The tracer-on drag data obtained in the BRL Transonic Range for the APIT, M20 projectile is listed in Table 8.

III. Results

The free flight spark range data were fitted to solutions of the linearized equations of motion and the resulting flight motion parameters were used to infer linearized aerodynamic coefficients, using the methods of Reference 4. Preliminary analysis of the aerodynamic data showed distinct variation of several coefficients with yaw level. In BRL Report 974, Murphy [5] has shown that aerodynamic coefficients derived from the linearized data reduction can be used to infer the coefficients in a nonlinear force and moment expansion, if sufficient data are available. For the caliber .50 bullets, sufficient data were obtained to permit determination of several nonlinear coefficients. A more detailed analysis of nonlinear effects is presented in the subtopics of this section, which discuss individual aerodynamic coefficients.

1. Drag Coefficient

The drag coefficient, C_D, is determined by fitting the time-distance measurements from the range flight. C_D is distinctly nonlinear with yaw level, and the value determined from an individual flight reflects both the zero-yaw drag coefficient, C_{D_0}, and the induced drag due to the average yaw level of the flight. The drag coefficient variation is expressed as an even power series in yaw amplitude:

$$C_D = C_{D_0} + C_{D_{\delta^2}} \delta^2 + \ldots \qquad (1)$$

where C_{D_0} is the zero-yaw drag coefficient, $C_{D_{\delta^2}}$ is the quadratic yaw-drag coefficient, and δ^2 is the total angle of attack squared.

Preliminary analysis of the drag coefficient data for the three caliber .50 projectiles showed that the zero-yaw drag coefficients were, for practical purposes, identical. The drag data for all three round types were therefore combined, and a single yaw-drag curve was determined. No significant variation of the yaw-drag coefficient with projectile type could be found, and the yaw-drag curve shown in Figure 22 was used to correct all the range values of C_D to zero-yaw conditions.

Figures 19 through 21 illustrate the variation of C_{D_0} with Mach number for the three caliber .50 bullets. The zero-yaw drag coefficients for the Ball, M33; API, M8; and APIT, M20 (Tracer off) are essentially identical at all speeds tested. The round-to-round standard deviation in zero-yaw drag coefficient is 1.3 percent at supersonic speeds, for all bullet types.

Figure 21 also illustrates the effect of the burning tracer on the zero-yaw drag coefficient of the M20 projectile. The tracer adds heat and mass flux into the wake, which raises the base pressure and lowers the base drag. For the APIT, M20 projectile, the tracer reduces the total zero-yaw drag coefficient by approximately 7 percent, at all speeds tested.

Figure 23 is a comparison of the API, M8 drag coefficient obtained by H. P. Hitchcock [1] with the current Aerodynamics Range test results for the same projectile. Hitchcock's curve was converted from the old K_D to the modern C_D nomenclature [$C_D = (8/\pi) K_D$], and was also corrected for the difference in reference diameter (Hitchcock used 0.50 inch, and the present tests use 0.51 inch). Hitchcock's drag coefficient averages about 4 percent lower than the spark range curve at supersonic speeds, and about 10 percent higher at transonic and subsonic speeds. Considering the relatively crude instrumentation used in the 1943 resistance firings, the agreement is satisfactory.

2. Overturning Moment Coefficient

The range values of the overturning moment coefficient, C_{M_α}, were fitted using the appropriate squared-yaw parameters from Reference 5. A weak dependence of C_{M_α} on yaw level was observed for the caliber .50 projectiles. The overturning moment is assumed to be cubic in yaw level, and the coefficient variation is given by:

$$C_{M_\alpha} = C_{M_{\alpha 0}} + C_2 \delta^2 + \dots \quad (2)$$

where $C_{M_{\alpha 0}}$ is the zero-yaw overturning moment coefficient, and C_2 is the cubic coefficient.

Figure 27 illustrates the observed variation of C_2 with Mach number, and this curve was used to correct all the range values of C_{M_α} to zero-yaw conditions. Figures 24 through 26 show the variation of $C_{M_{\alpha 0}}$ with Mach number for the three caliber .50 projectiles. The Ball, M33 has the highest overturning moment coefficient of the three bullets; $C_{M_{\alpha 0}}$ for the API, M8 averages about 2 percent lower than that of the Ball, M33 and the APIT, M20 curve is approximately 10 percent lower than the Ball, M33 curve.

3. Gyroscopic Stability

The launch gyroscopic stability factors of the three caliber .50 bullets, fired from a barrel with 15 inch twist of rifling, at a muzzle velocity of 2950 feet/second, into a sea-level ICAO standard atmosphere, are as follows:

Projectile	Launch Gyroscopic Stability Factor
Ball, M33	1.8
API, M8	1.9
APIT, M20	2 2

A gyroscopic stability factor above 1.5 is usually considered adequate, so all the caliber .50 projectiles tested have sufficient gyroscopic stability to permit satisfactory flight in all expected conditions. including extreme cold weather (high air density) conditions. Since the caliber .50 ammunition is never fired at reduced muzzle velocities, the lower values of S_g observed in Tables 5 through 7 will never occur in field firings.

4. Lift Force Coefficient

The range values of the lift force coefficient, C_{L_α}, were also analyzed using the methods of Reference 5. A weak dependence of C_{L_α} on yaw level was observed for the caliber .50 projectiles. The variation of C_{L_α} with yaw level is also assumed to be cubic:

$$C_{L_\alpha} = C_{L_{\alpha 0}} + a_2 \delta^2 + \dots \quad (3)$$

where $C_{L_{\alpha 0}}$ is the zero-yaw lift force coefficient, and a_2 is the cubic coefficient.

Figure 31 illustrates the variation of the cubic lift force coefficient with Mach number. The subsonic and supersonic regions showed distinctly different levels of cubic behavior, and the curve of Figure 31 was used to correct all range values of C_{L_α} to zero-yaw conditions.

The variation of $C_{L_{\alpha 0}}$ with Mach number for the three caliber .50 bullets is shown in Figures 28 through 30. The zero-yaw lift force coefficients of the three projectiles are essentially identical.

5. Magnus Moment Coefficient and Pitch Damping Moment Coefficient

The Magnus moment coefficient, $C_{M_{p\alpha}}$, and the pitch damping moment coefficient sum $(C_{M_q} + C_{M_{\dot\alpha}})$, are discussed together, since if either coefficient is nonlinear with yaw level, both coefficients exhibit nonlinear coupling in the data reduction process.[5] Due to mutual reaction, the analysis of $C_{M_{p\alpha}}$ and $(C_{M_q} + C_{M_{\dot\alpha}})$ must be performed simultaneously, even though the aerodynamic moments are not, in themselves, directly physically related.

If the dependence of the Magnus moment and the pitch damping moment are cubic in yaw level, the nonlinear variation of the two moment coefficients is of the general form:

$$C_{M_{p\alpha}} = C_{M_{p\alpha 0}} + \hat{C}_2 \delta^2 \quad (4)$$

$$\left(C_{M_q} + C_{M_{\dot\alpha}}\right) = \left(C_{M_q} + C_{M_{\dot\alpha}}\right)_0 + d_2 \delta^2 \quad (5)$$

where $C_{M_{p\alpha 0}}$ and $\left(C_{M_q} + C_{M_{\dot\alpha}}\right)_0$ are the zero-yaw values of Magnus and pitch damping moment coefficients, respectively, and $\hat{C}_2$ and d_2 are the associated cubic coefficients.

In Reference 5, it is shown that the nonlinear coupling introduced through the least squares fitting process yields the following expressions for range values [R-subscript] of $C_{M_{p\alpha}}$ and $\left(C_{M_q} + C_{M_{\dot\alpha}}\right)$:

$$\left[C_{M_{p\alpha}}\right]_R = C_{M_{p\alpha 0}} + \hat{C}_2 \delta_\epsilon^2 + d_2 \delta_{\epsilon TH}^2 \quad (6)$$

$$\left[\left(C_{M_q} + C_{M_{\dot\alpha}}\right)\right]_R = \left(C_{M_q} + C_{M_{\dot\alpha}}\right)_0 + \hat{C}_2 \delta_{\epsilon HH}^2 + d_2 \delta_{\epsilon HT}^2 \quad (7)$$

where the above effective squared yaws are defined as:

$$\delta_\epsilon^2 = K_F^2 + K_S^2 + \frac{(\phi_F' K_F^2 - \phi_S' K_S^2)}{(\phi_F' - \phi_S')} \quad (8)$$

$$\delta_{\epsilon TH}^2 = \left(\frac{I_x}{I_y}\right)\left[\frac{(K_F^2 \phi_F'^2 - K_S^2 \phi_S'^2)}{(\phi_F'^2 - \phi_S'^2)}\right] \quad (9)$$

$$\delta^2_{e_{HH}} = \left(\frac{I_y}{I_x}\right)\left[\frac{(\phi'_F + \phi'_S)(K_S^2 - K_F^2)}{(\phi'_F - \phi'_S)}\right] \quad (10)$$

$$\delta^2_{e_{HT}} = \frac{(\phi'_F K_S^2 - \phi'_S K_F^2)}{(\phi'_F - \phi'_S)} \quad (11)$$

The remaining symbols are defined in the List of Symbols in this report.

Preliminary analysis of the caliber .50 data indicated strong nonlinearity in the range values of $C_{M_{p\alpha}}$ and $(C_{M_q} + C_{M_\alpha})$ at angles of attack less than 3 degrees, but essentially no variation of either coefficient was observed at larger yaw levels. The data rounds were separated into Mach number groups, and an analysis was performed to determine the cubic coefficients at both small and large yaw levels. No significant values of the cubic pitch damping moment coefficient, d_2 , could be found.

Figures 32 through 34 illustrate the variation of the range values of $C_{M_{p\alpha}}$ with the appropriate squared yaw parameter from Reference 5. The general characteristic of these plots is bi-cubic behavior, with strong nonlinearity at small yaw levels, followed by no significant variation of $C_{M_{p\alpha}}$ with yaw level at larger yaws. The small-yaw cubic Magnus moment coefficient varies significantly with Mach number, but the large-yaw $C_{M_{p\alpha}}$ appears to be essentially independent of Mach number at supersonic speeds.

Least squares fitting of the Magnus moment coefficient data yielded the curve of Figure 38 for $\hat{C}_2$, which was then used to correct the range values of $C_{M_{p\alpha}}$ and $C_{M_q} + C_{M_\alpha}$ to zero-yaw conditions. Figures 35 through 37 show the variation of $C_{M_{p\alpha_0}}$ with Mach number for the three caliber .50 bullets, and Figures 39 through 41 illustrate the variation of $\left(C_{M_q} + C_{M_{\dot\alpha}}\right)_0$ with Mach number.

It should be noted that the analysis of nonlinear Magnus and pitch damping moment data from free flight spark ranges is a delicate process at best, and the results are highly sensitive to small errors in determination of the damping exponents on the two modal arms. The uncertainties in damping rate determinations are reflected in the larger round-to-round data scatter in Magnus and pitch damping moment coefficients, compared with the smaller scatter observed in the overturning moment coefficients.

6. Damping Rates

The damping rates, λ_F and λ_S , of the fast and slow yaw modes indicate the dynamic stability of a projectile. Negative λ's indicate damping; a positive λ means that its associated modal arm will grow with increasing distance along the trajectory.

For a projectile whose Magnus or pitch damping moments are nonlinear with yaw level, the damping rates also show a nonlinear dependence on yaw.[6] Figures 42 through 47 illustrate the variations in damping rates with yaw level for the three caliber .50 bullets at supersonic and subsonic speeds. Figures 42 and 43 show that both modal arms are damped at all yaw levels tested, for high supersonic speeds. At low supersonic speeds. Figures 44 and 45 shows a damped fast arm at all yaw levels tested, but the slow arm is unstable at small yaw and stable at larger yaw levels. This behavior is described by the aeroballistician as limit-cycle yaw, and Figure 45 predicts a slow arm limit-cycle yaw of about 3 degrees at low supersonic and transonic speeds.

Figures 46 and 47 show the variation of the fast and slow arm damping rates with yaw level at subsonic speeds, for the three caliber .50 bullets. The fast arm shows generally satisfactory damping for the Ball, M33 and API, M8 bullets at subsonic speeds, with very weak undamping of the fast arm observed for the APIT, M20 design. Figure 47 indicates a slow arm limit-cycle for all bullet types at subsonic speeds. The magnitude of the expected slow arm limit-cycle yaw at subsonic speeds is slightly greater than 4 degrees, for all three caliber .50 bullets.

IV. Conclusions

The drag coefficients of the caliber .50 Ball, M33, API, M8 and tracer-off APIT, M20 projectiles are essentially identical at all speeds tested. The effect of the burning tracer on the APIT, M20 is to reduce the tracer-off drag approximately 7 percent. The observed round-to-round standard deviation in drag coefficient is 1.3 percent at supersonic speeds, for all three bullet types.

The three caliber .50 bullets tested have sufficient gyroscopic stability to permit satisfactory flight at all conditions, including extreme cold weather (high air density), when fired at service velocity from a barrel with standard 381mm (15 inch) twist of rifling.

The non-linear Magnus moment characteristics of the three caliber .50 bullets predict a slow arm limit cycle yaw of approximately 3 degrees at low supersonic and transonic speeds. The low speed Magnus moment behavior predicts a slow arm limit cycle yaw slightly exceeding 4 degrees at subsonic speeds.

V. Recommendations

A long range limit cycle yaw test should be conducted with the caliber .50 service ammunition to verify the flight dynamic predictions made in this report.

A radar doppler velocimeter test should be conducted for the caliber .50 projectiles to verify the drag coefficient results out to long ranges, and very low subsonic speeds.

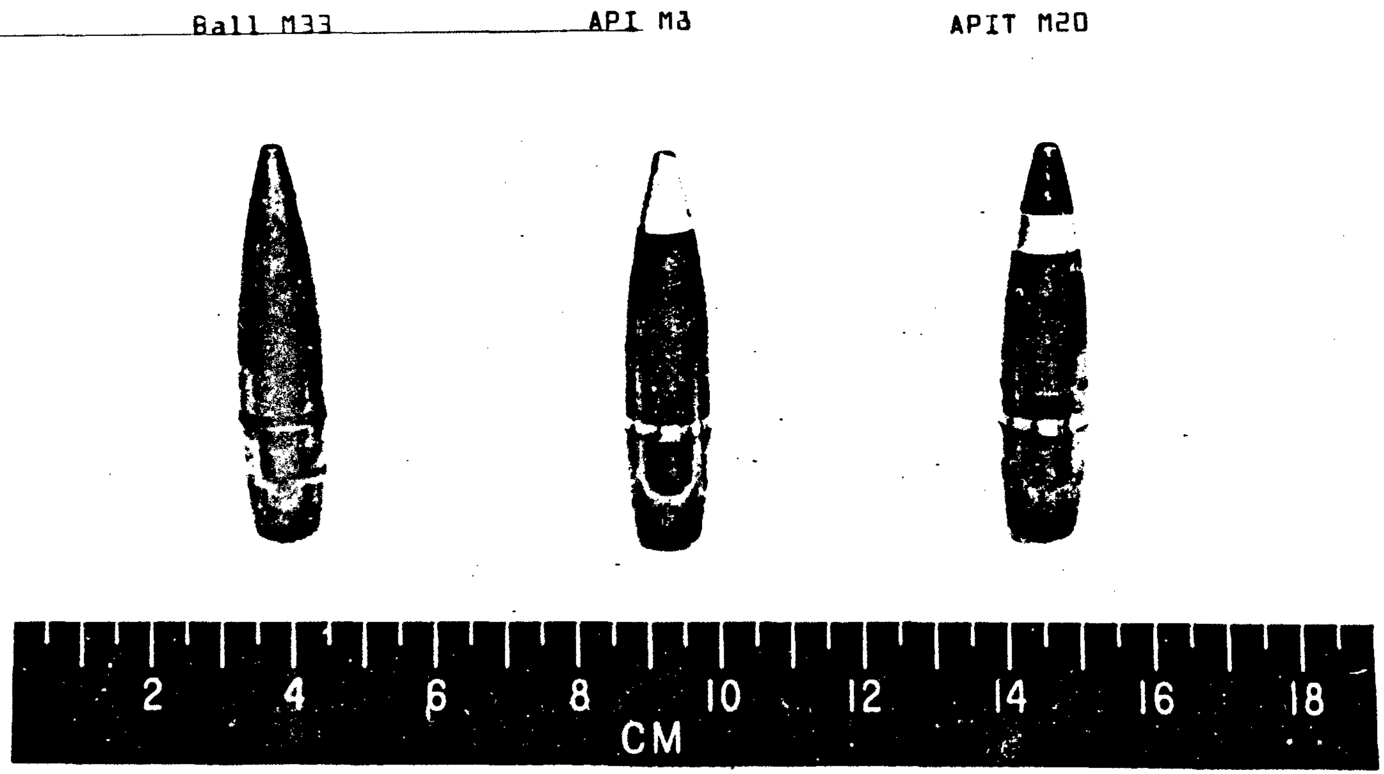

Figure 1. Photograph of the Caliber .50 Projectiles.

Figure 2. Photograph of the BRL Free Flight Aerodynamics Range.

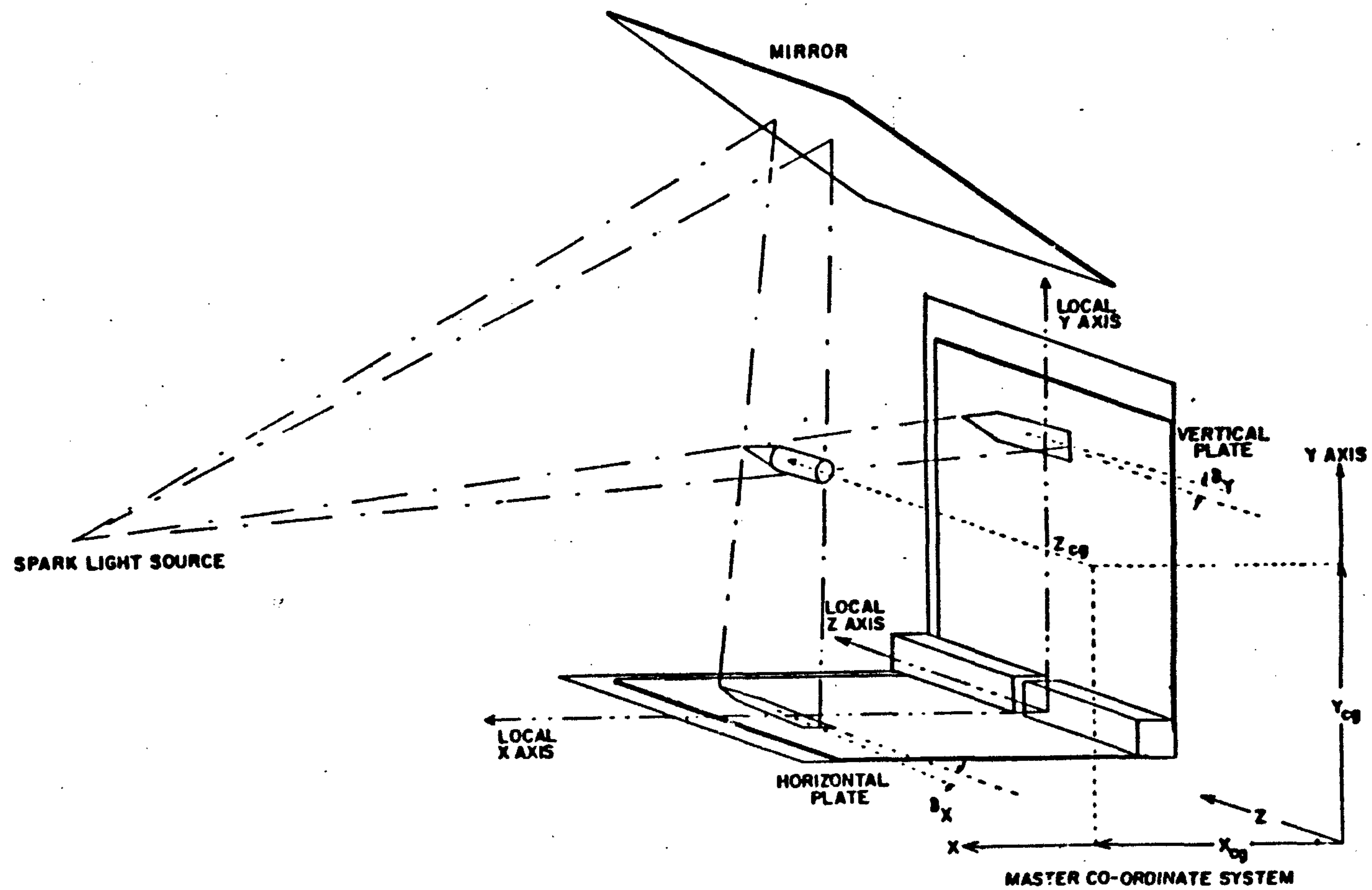

Figure 3. Coordinate System for the BRL Aerodynamics Range.

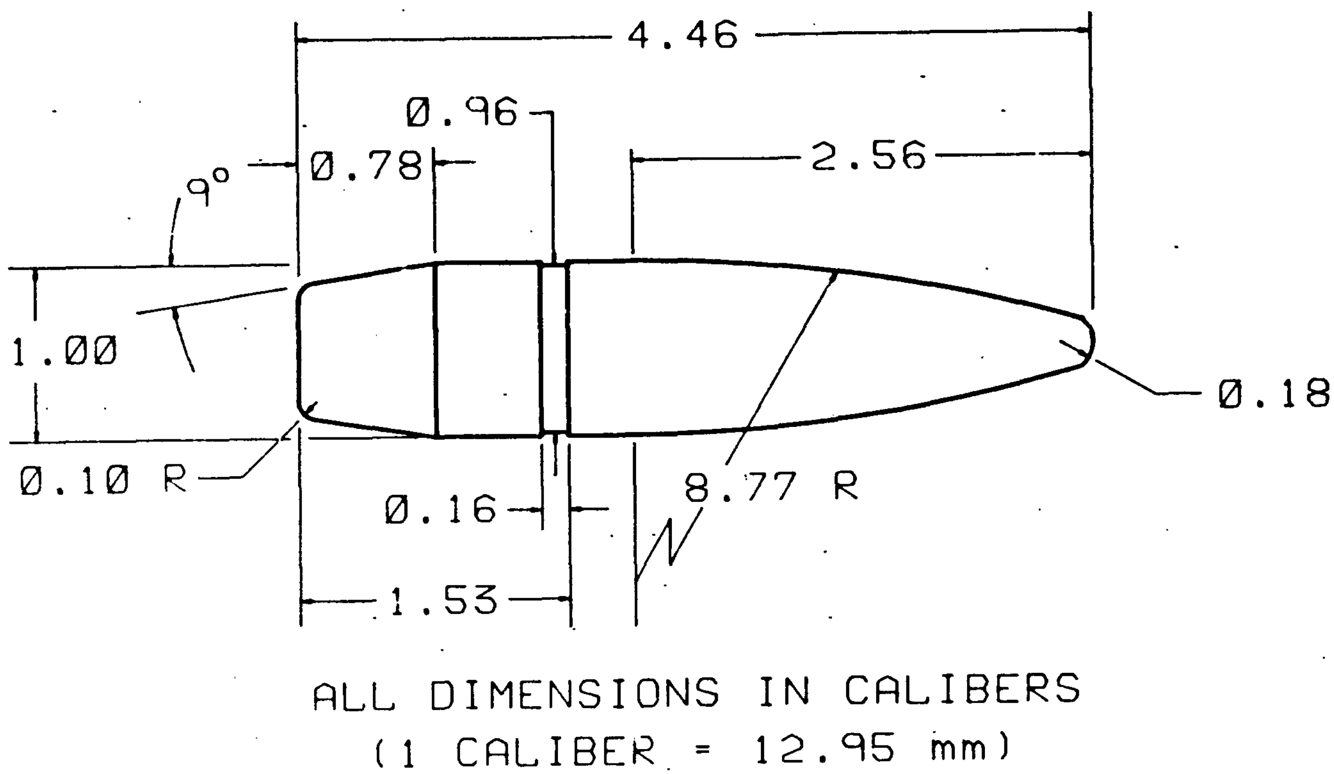

Figure 4. Sketch of the Caliber .50 Projectiles.

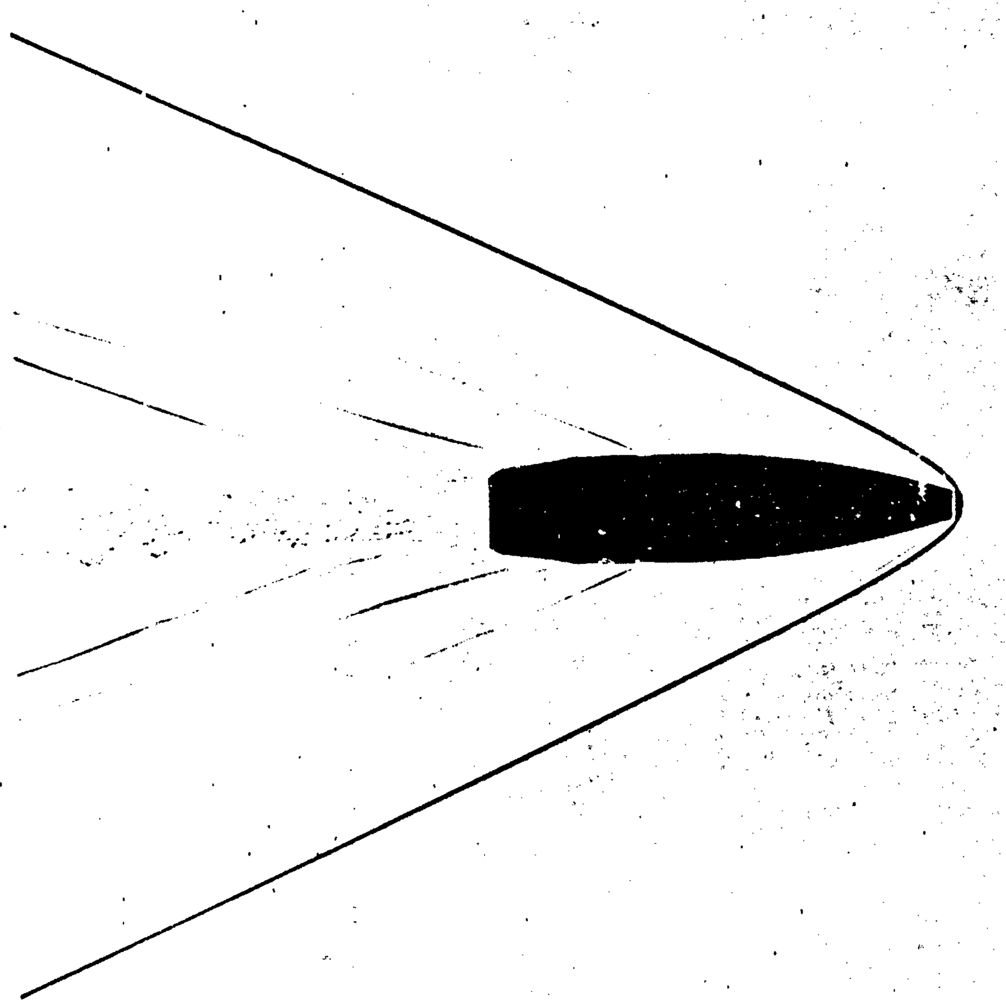

Figure 5. Shadowgraph of Ball, M33 Projectile at Mach 2.66.

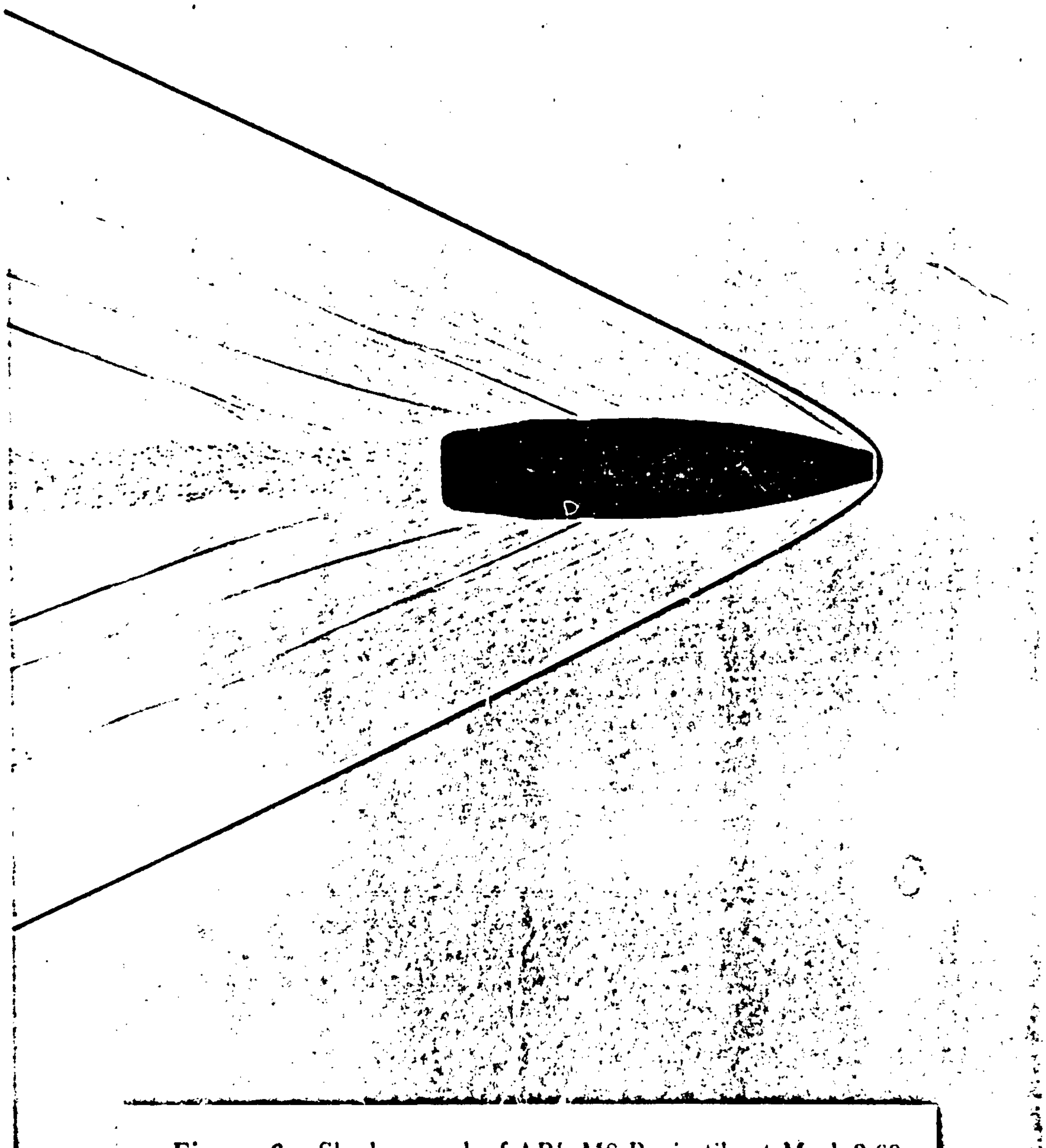

Figure 6. Shadowgraph of API M8 Projectile at Mach 2.60.

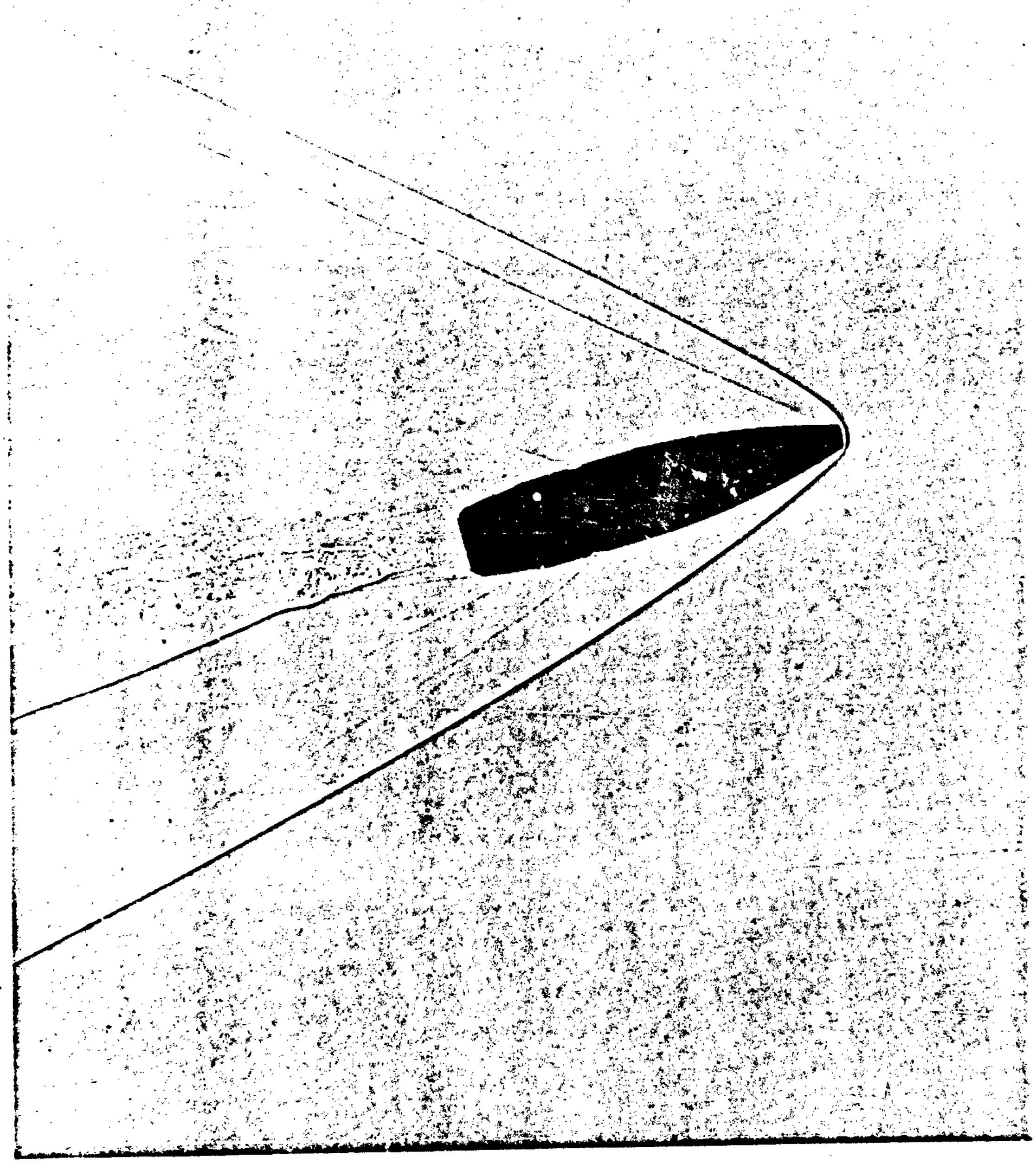

Figure 7. Shadowgraph of API, M8 Projectile at Mach 2.60, Angle of Attack = 15.4 Degrees.

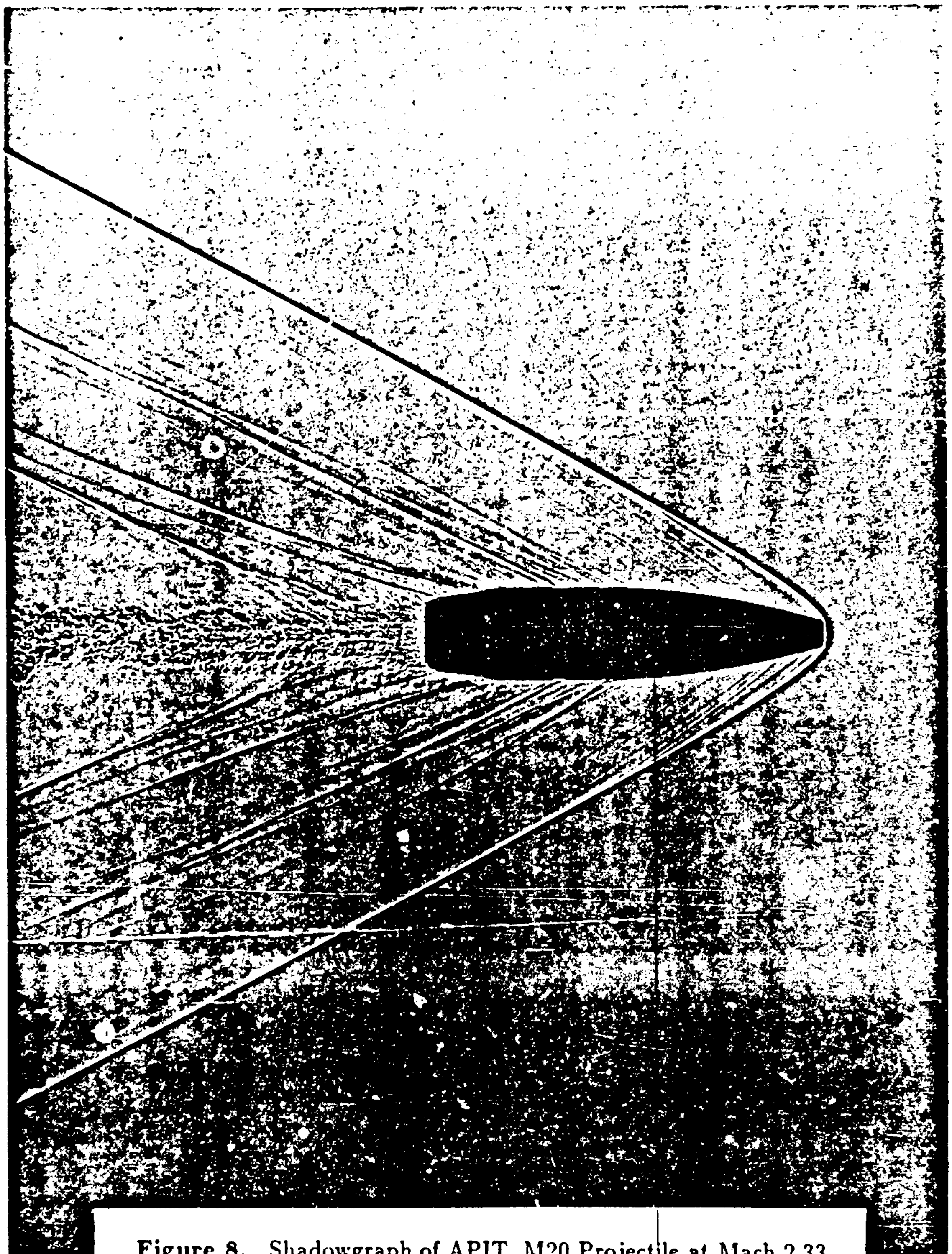

Figure 8. Shadowgraph of APIT, M20 Projectile at Mach 2.33.

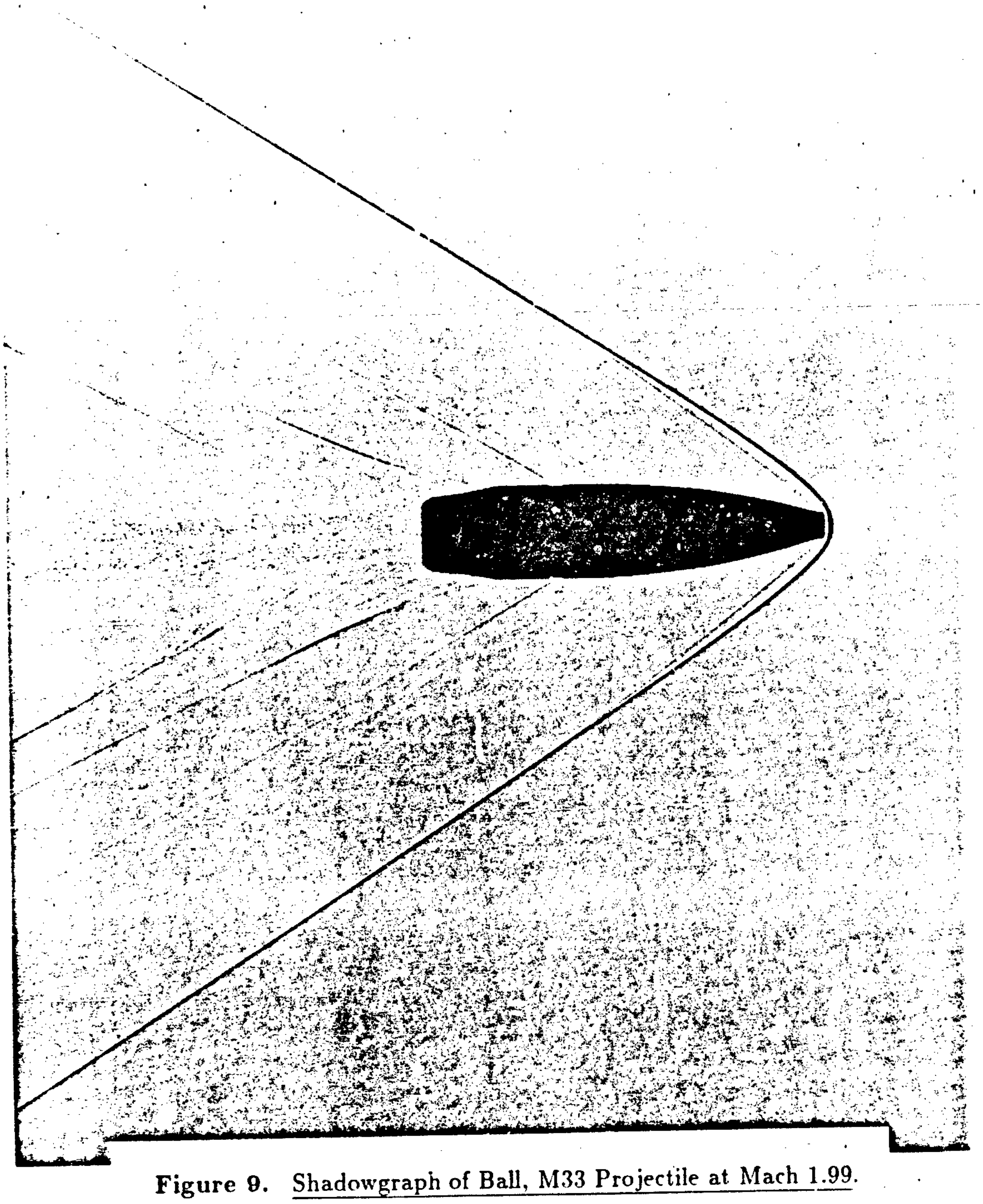

Figure 9. Shadowgraph of Ball, M33 Projectile at Mach 1.99.

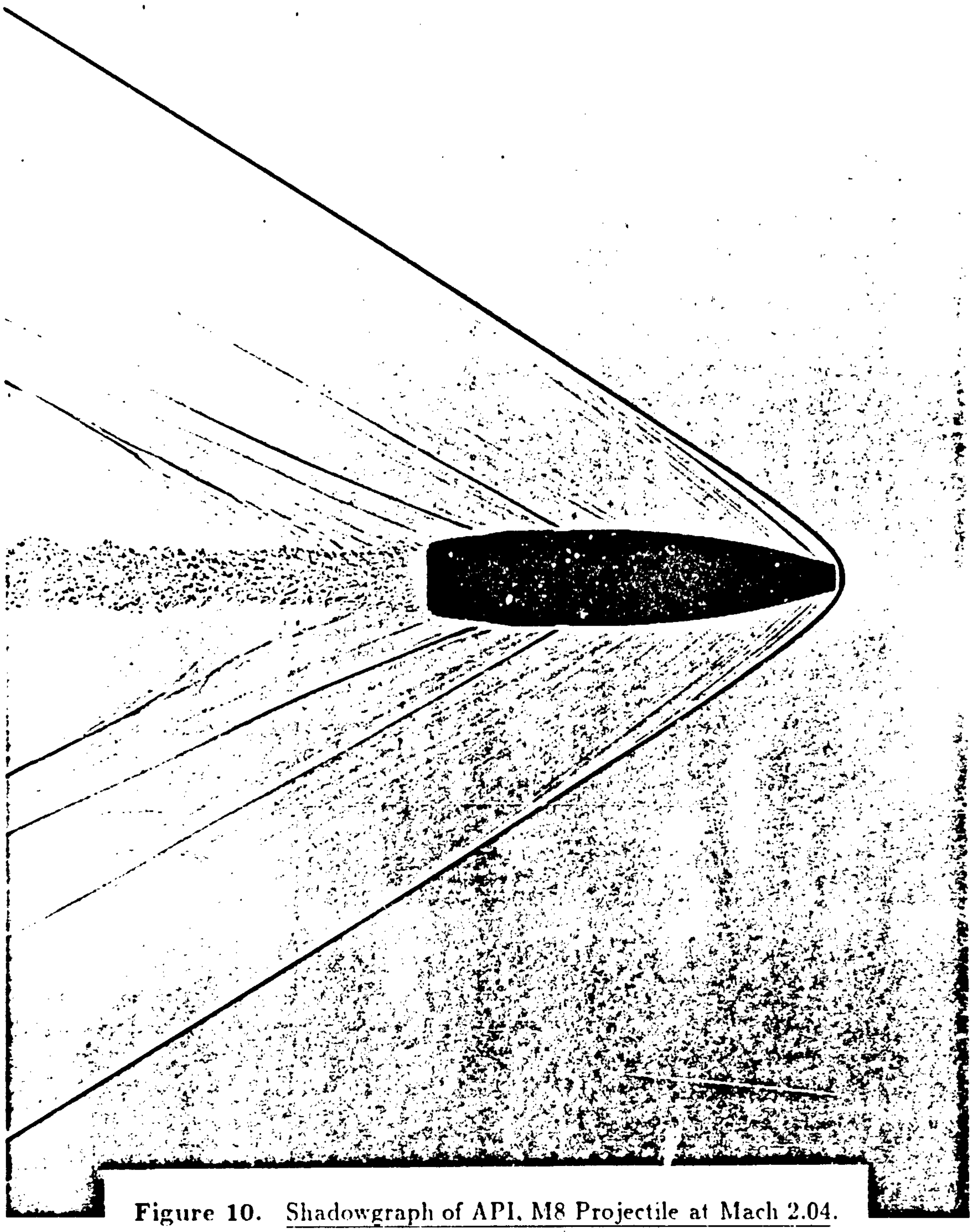

Figure 10. Shadowgraph of API, M8 Projectile at Mach 2.04.

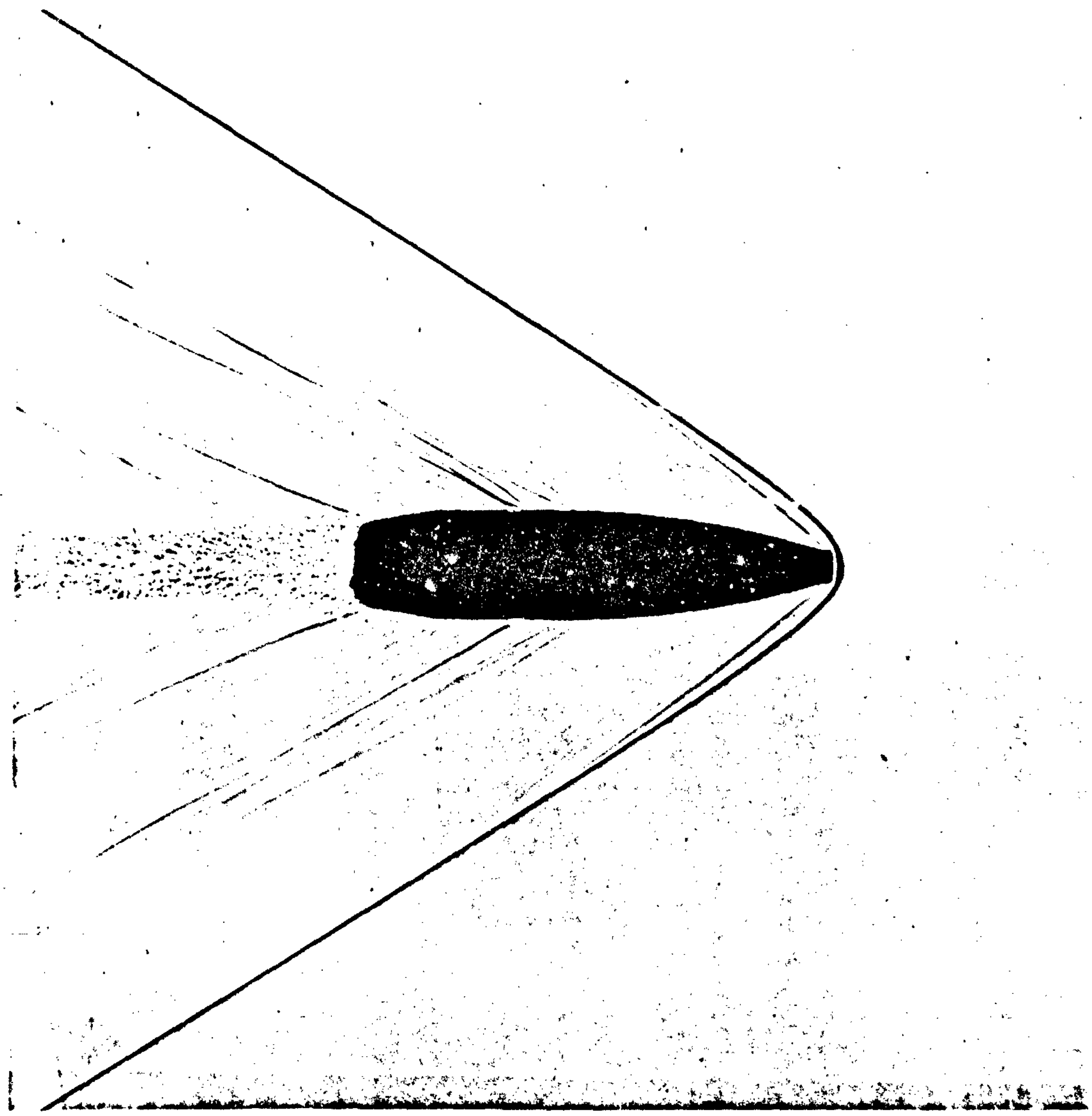

Figure 11. Shadowgraph of APIT, M20 Projectile at M.-h 2.01.

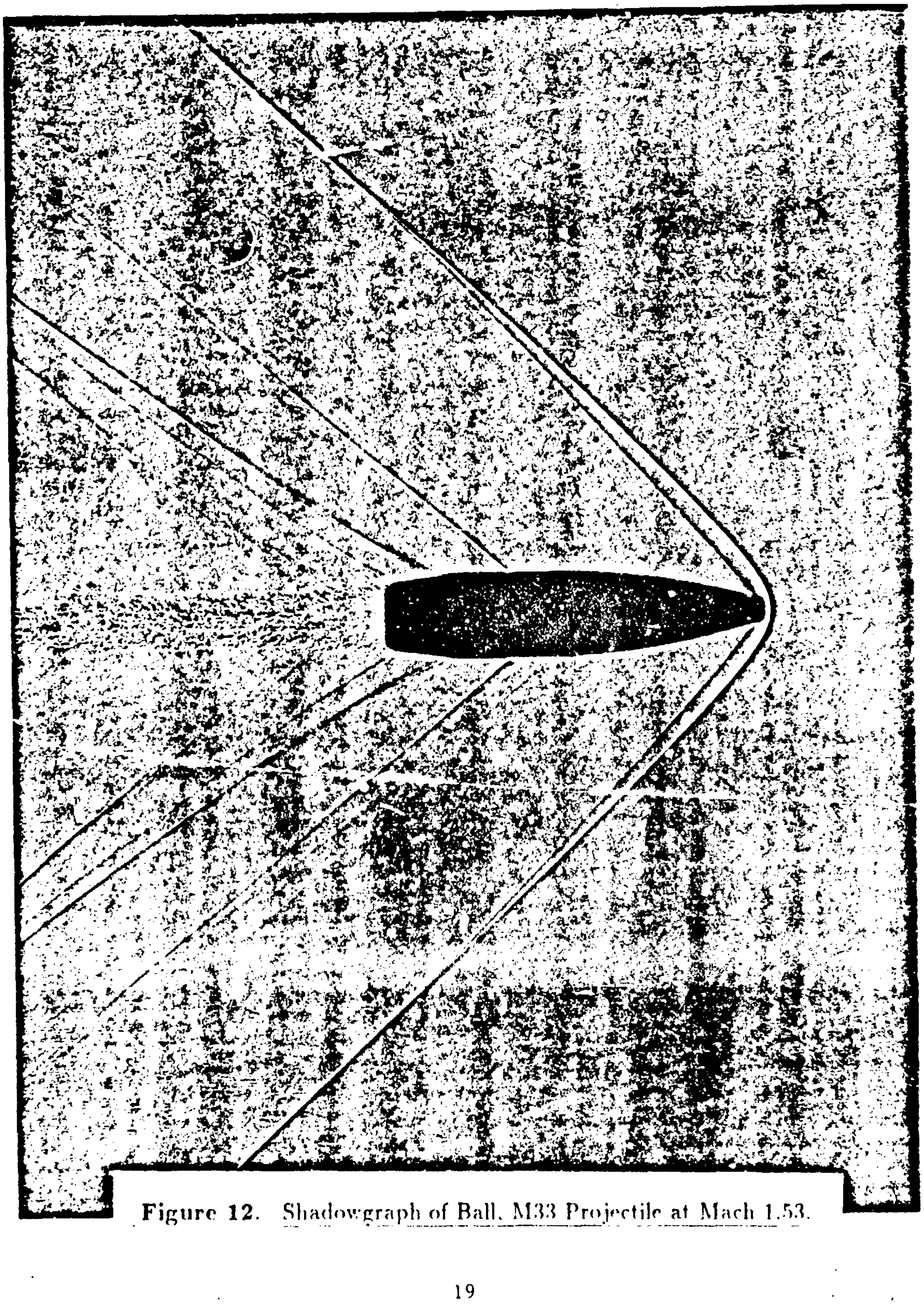

Figure 12. Shadowgraph of Ball, M33 Projectile at Mach 1.53.

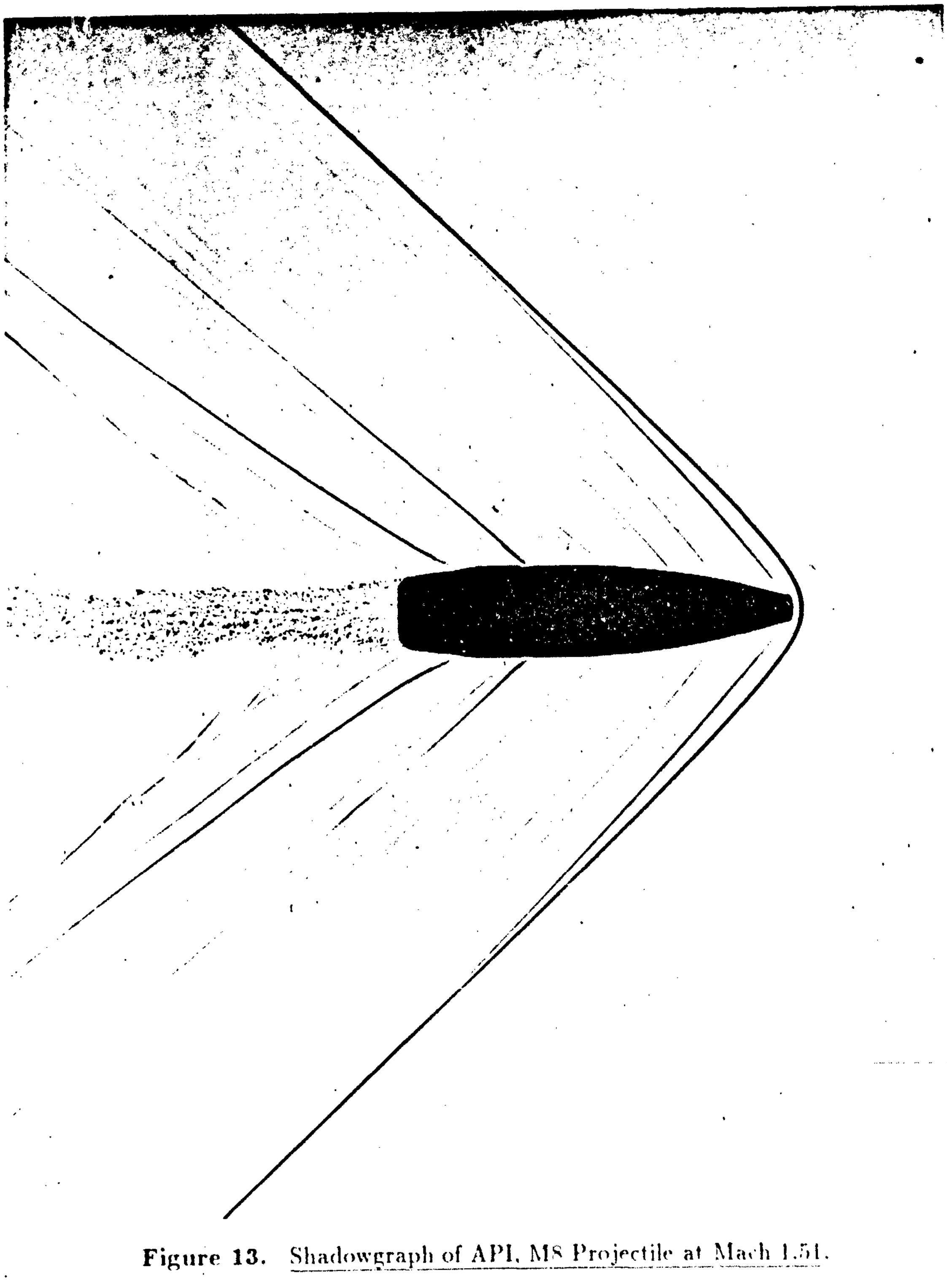

Figure 13. Shadowgraph of API, M8 Projectile at Mach 1.51.

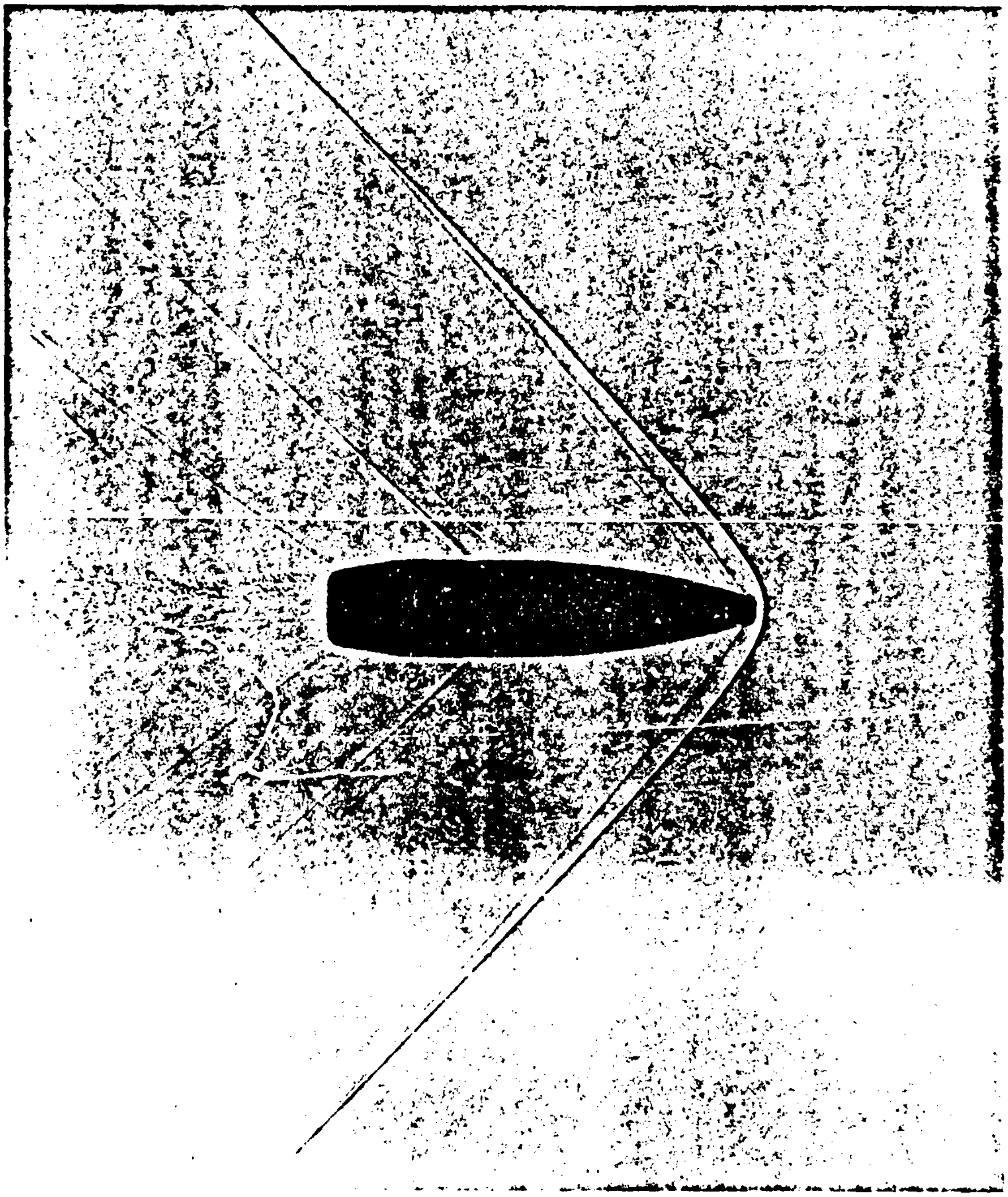

Figure 14. Shadowgraph of APIT, M20 Projectile at Mach 1.45.

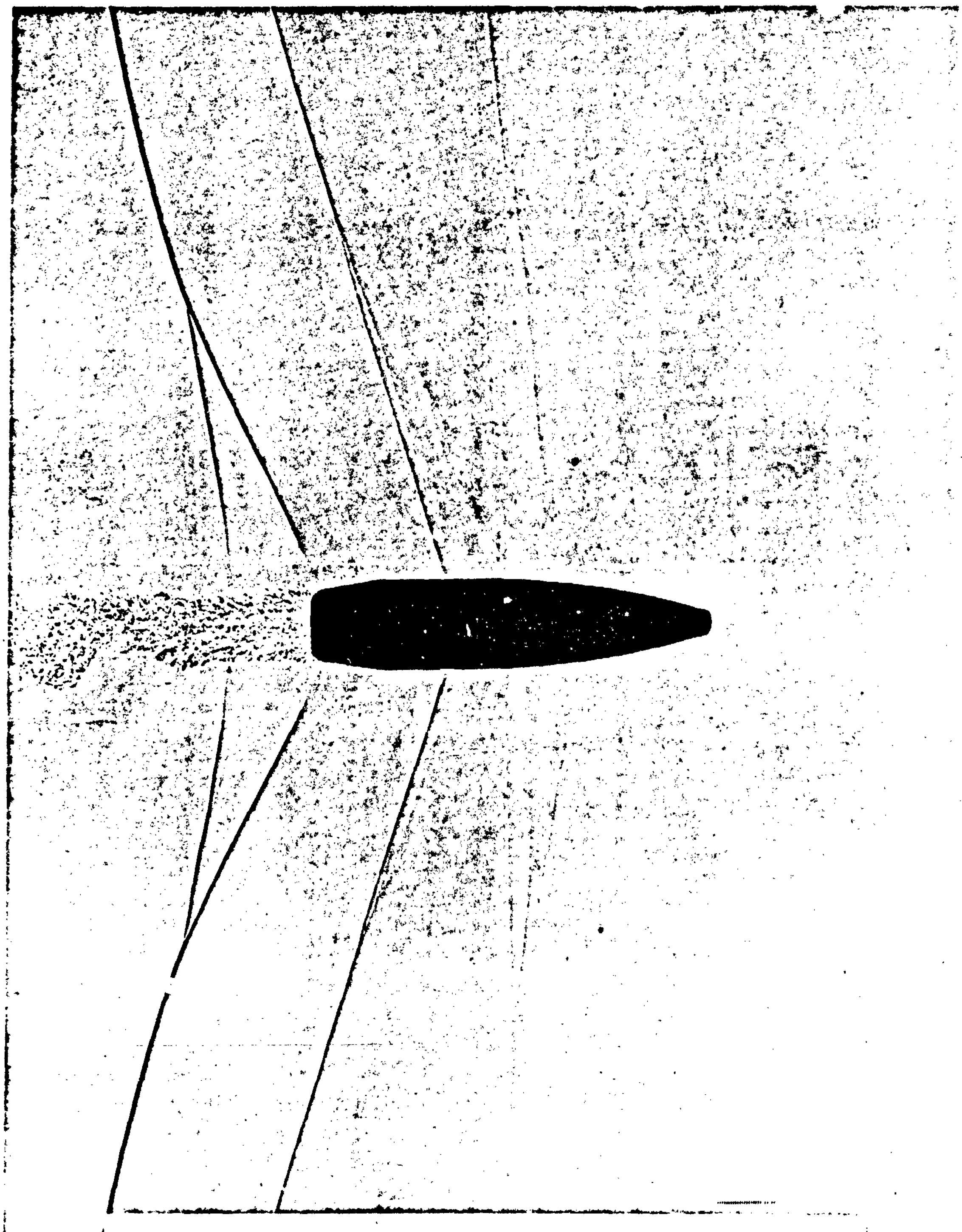

Figure 15. Shadowgraph of Ball, M33 Projectile at Mach 1.00.

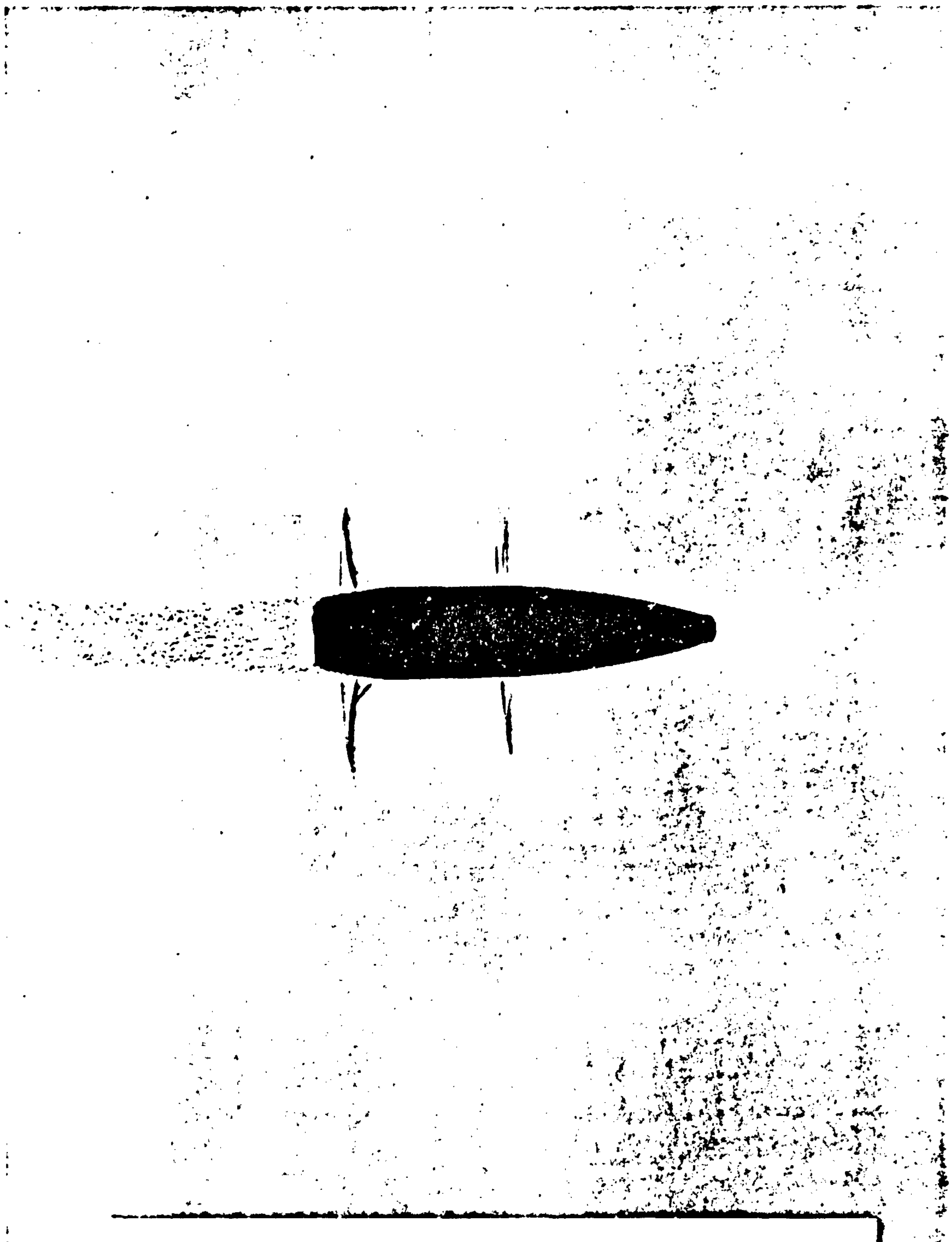

Figure 16. Shadowgraph of Ball, M33 Projectile at Mach 0.92.

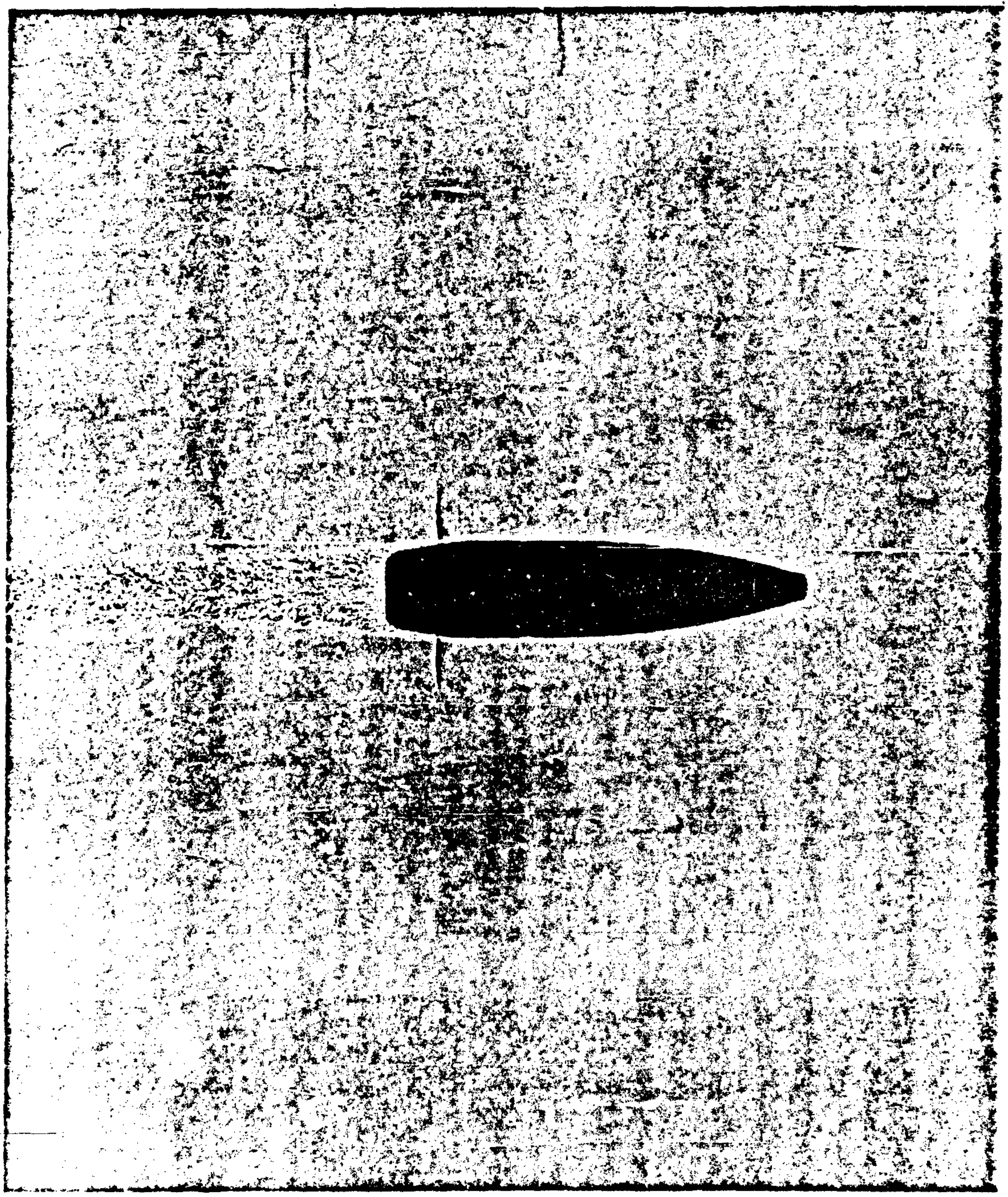

Figure 17. Shadowgraph of Ball, M33 Projectile at Mach 0.89.

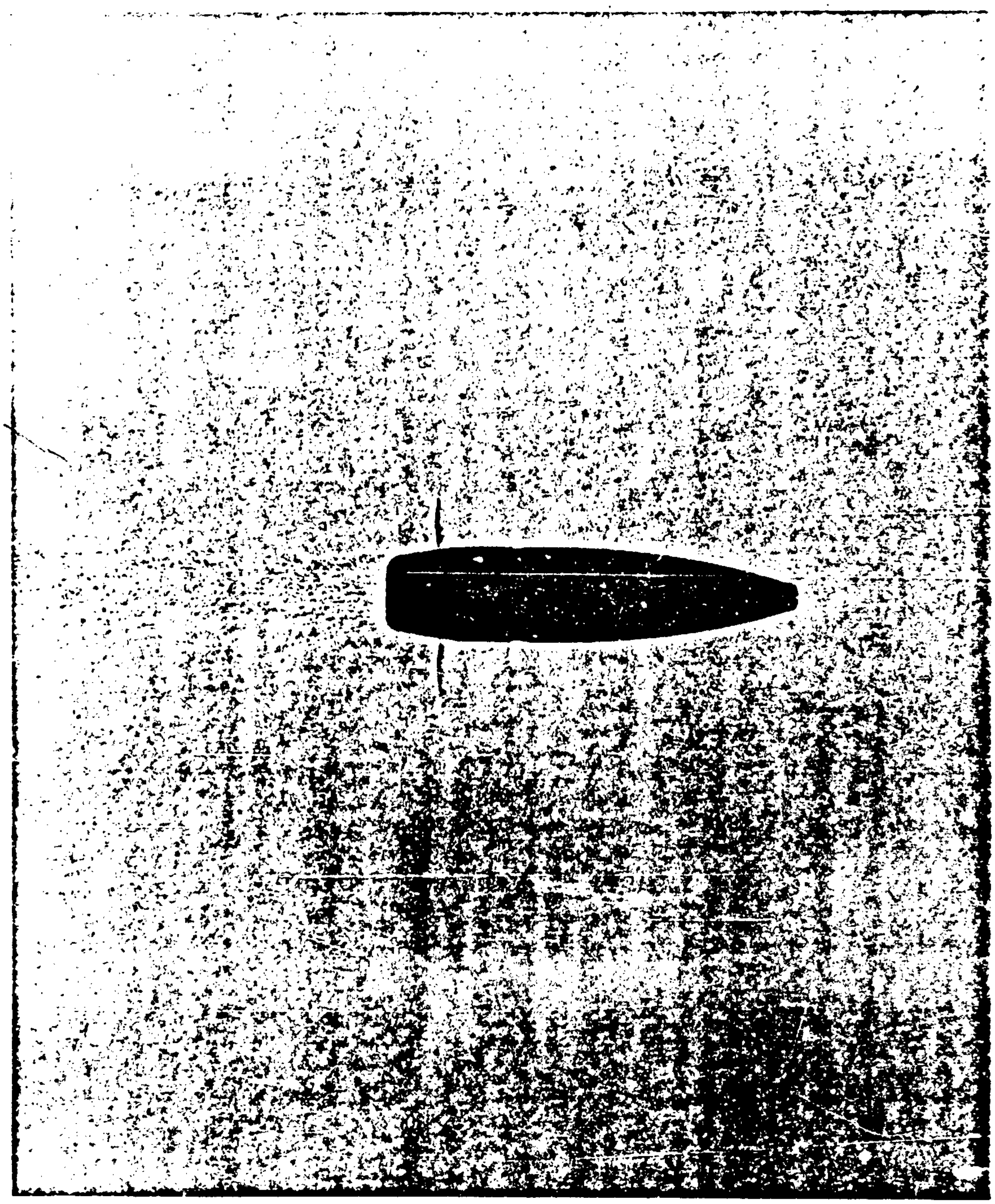

Figure 18. Shadowgraph of API, M8 Projectile at Mach 0.90.

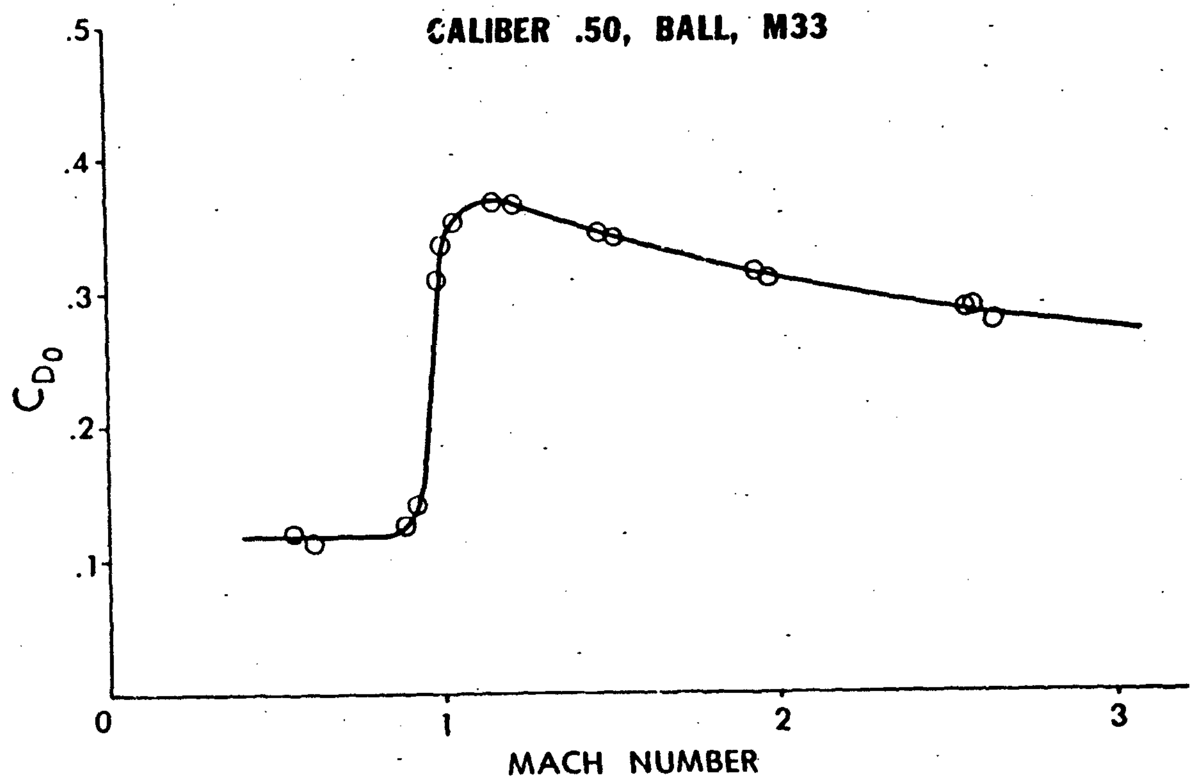

Figure 19. Zero-Yaw Drag Force Coefficient versus Mach Number, Ball, M33.

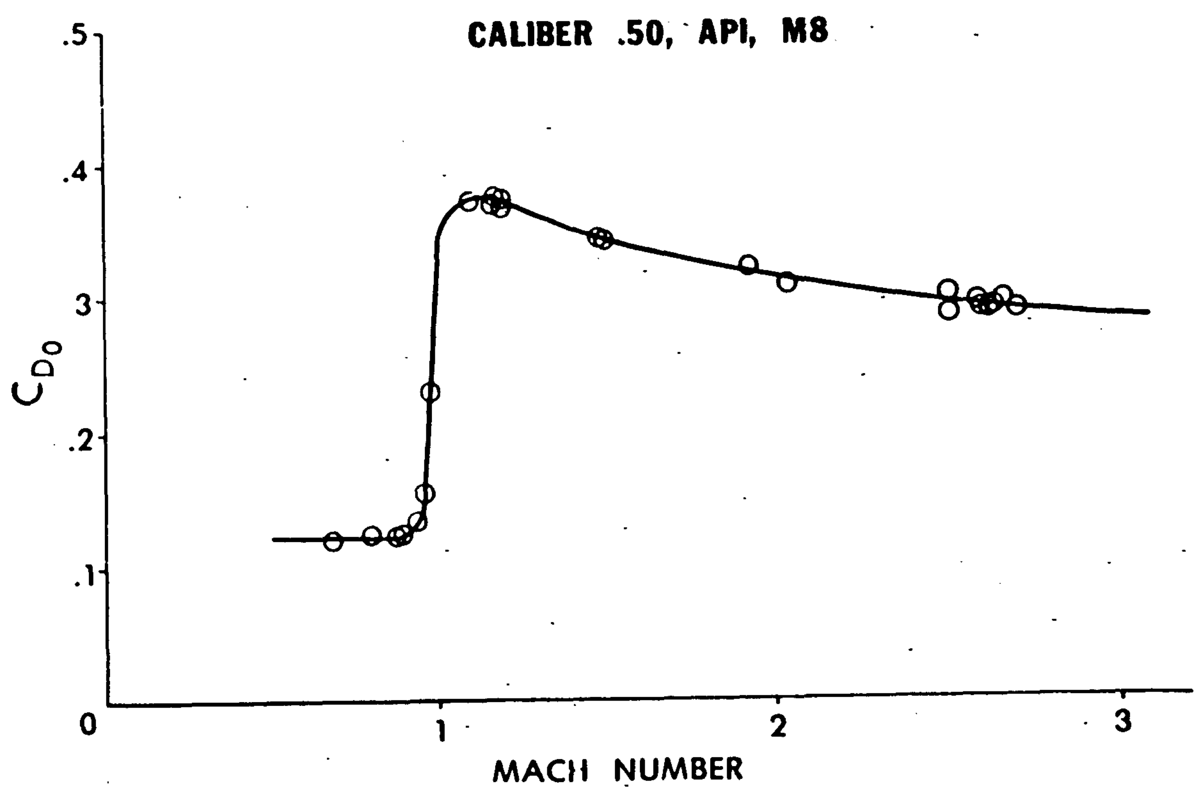

Figure 20. Zero-Yaw Drag Force Coefficient versus Mach Number, API, M8.

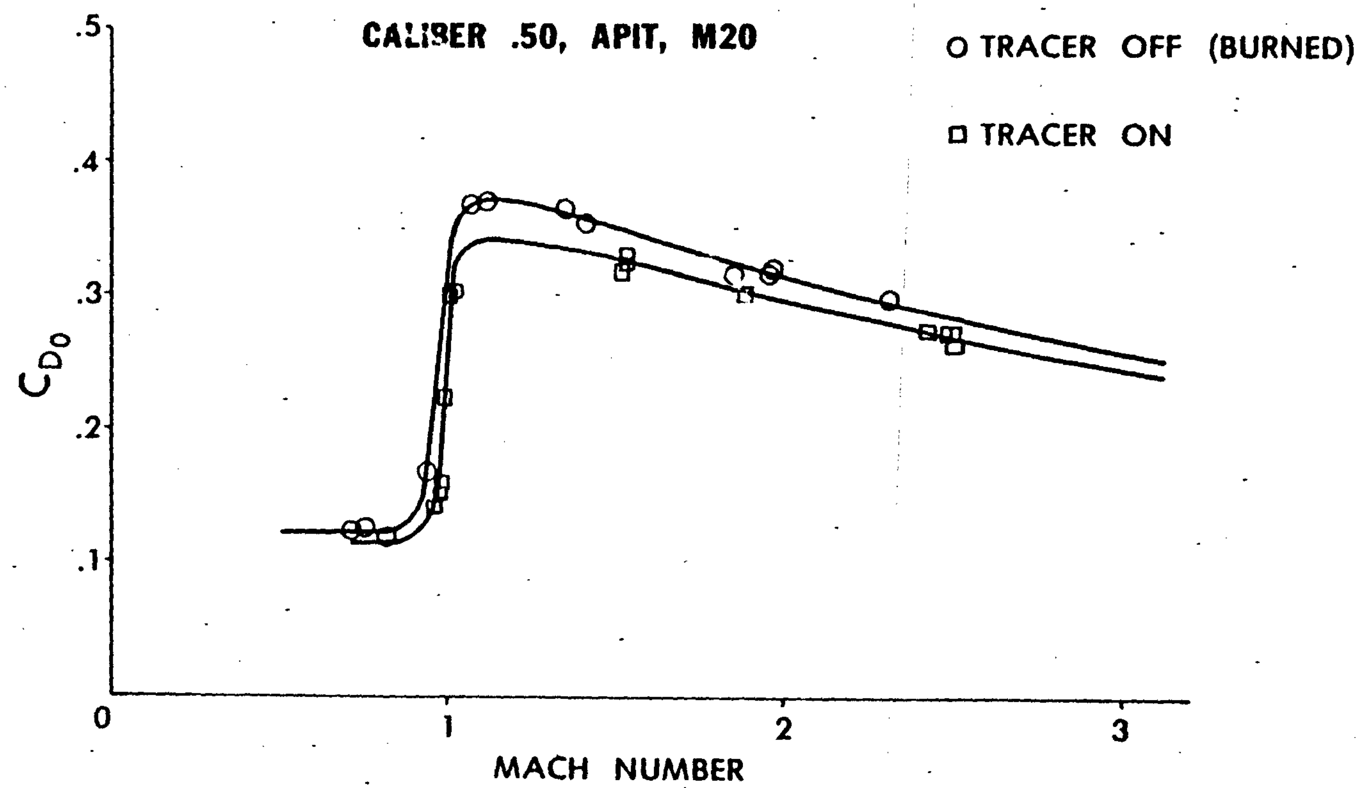

Figure 21. Zero-Yaw Drag Force Coefficient versus Mach Number, APIT, M20.

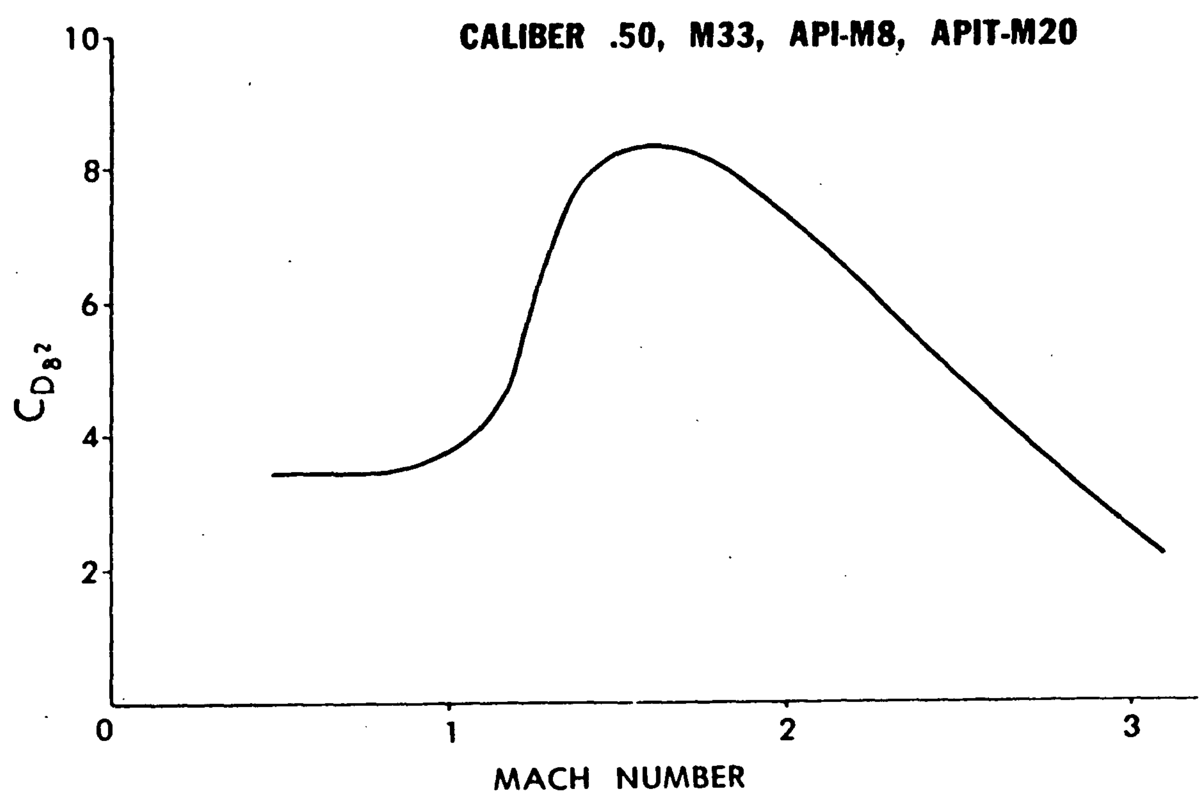

Figure 22. Yaw Drag Force Coefficient versus Mach Number

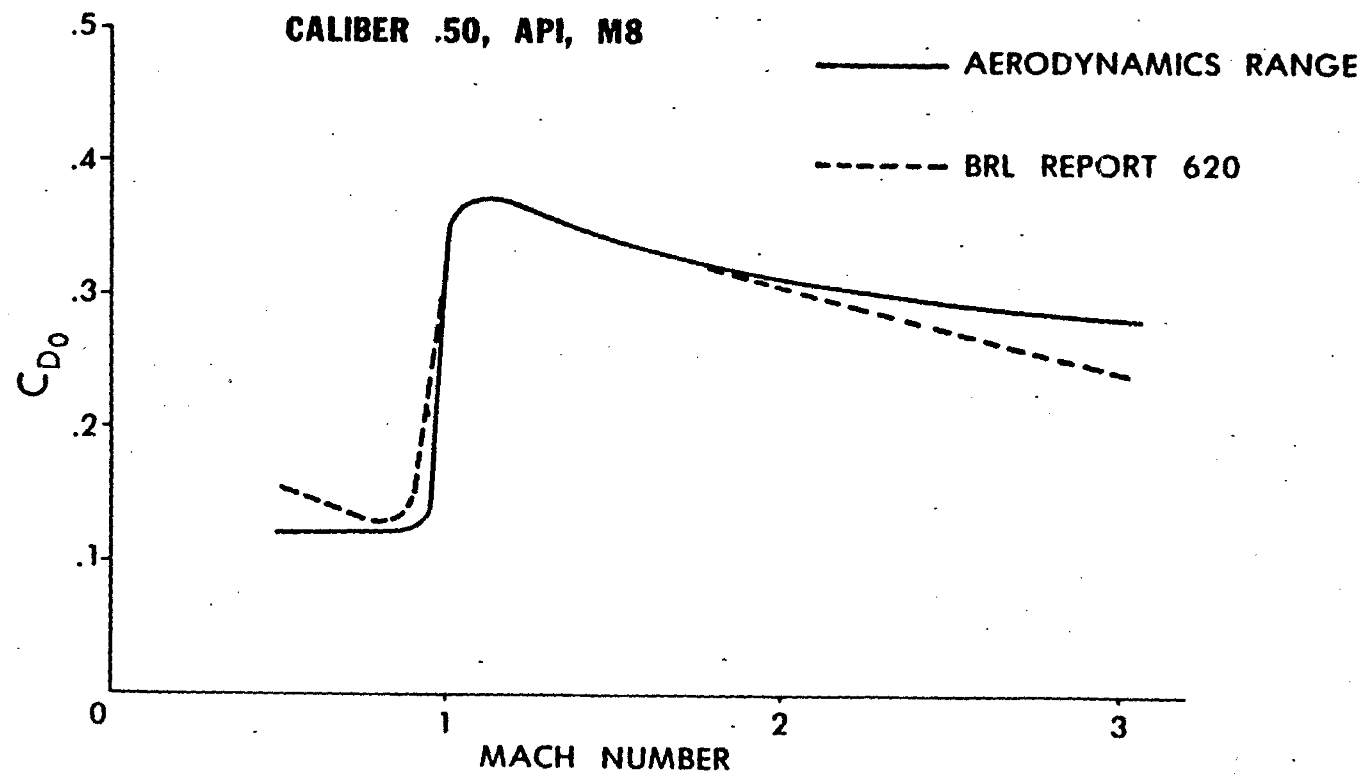

Figure 23. Comparison of Old and New Drag Coefficients for the API, M8 Projectile

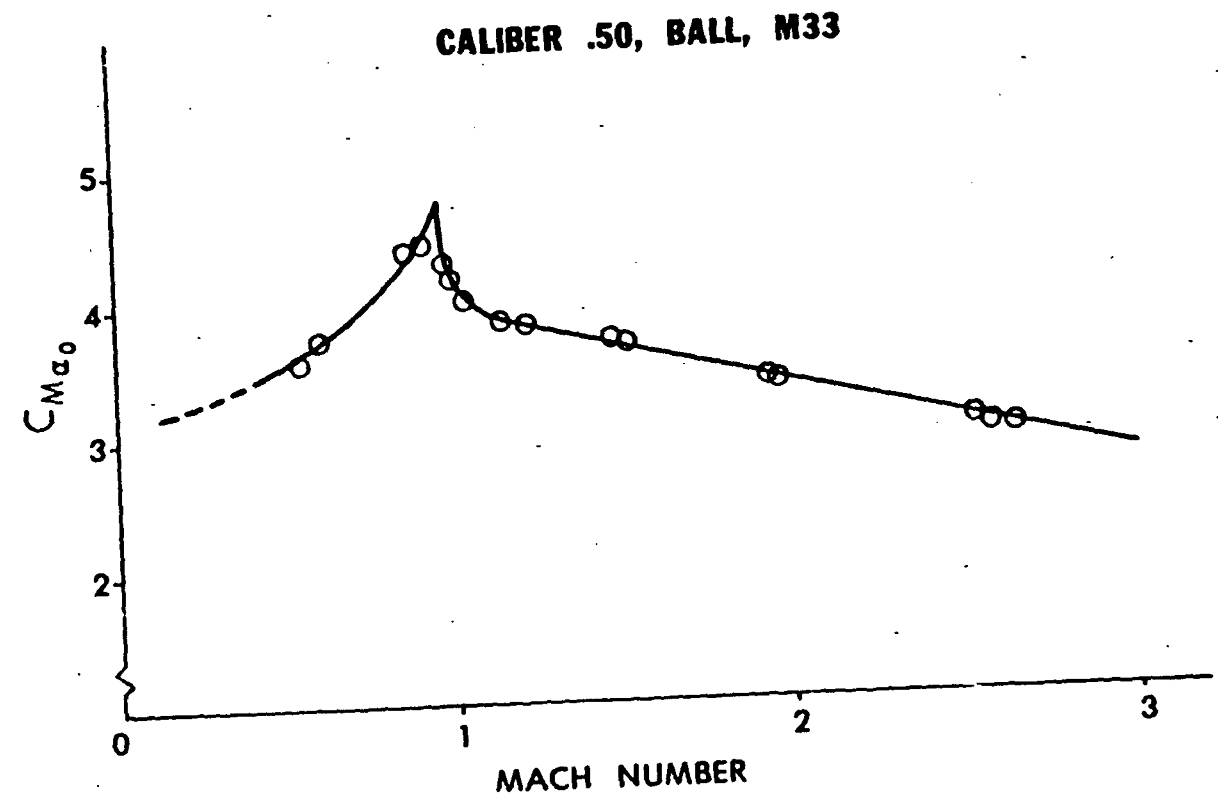

Figure 24. Zero-Yaw Overturning Moment Coefficient versus Mach Number, Ball, M33.

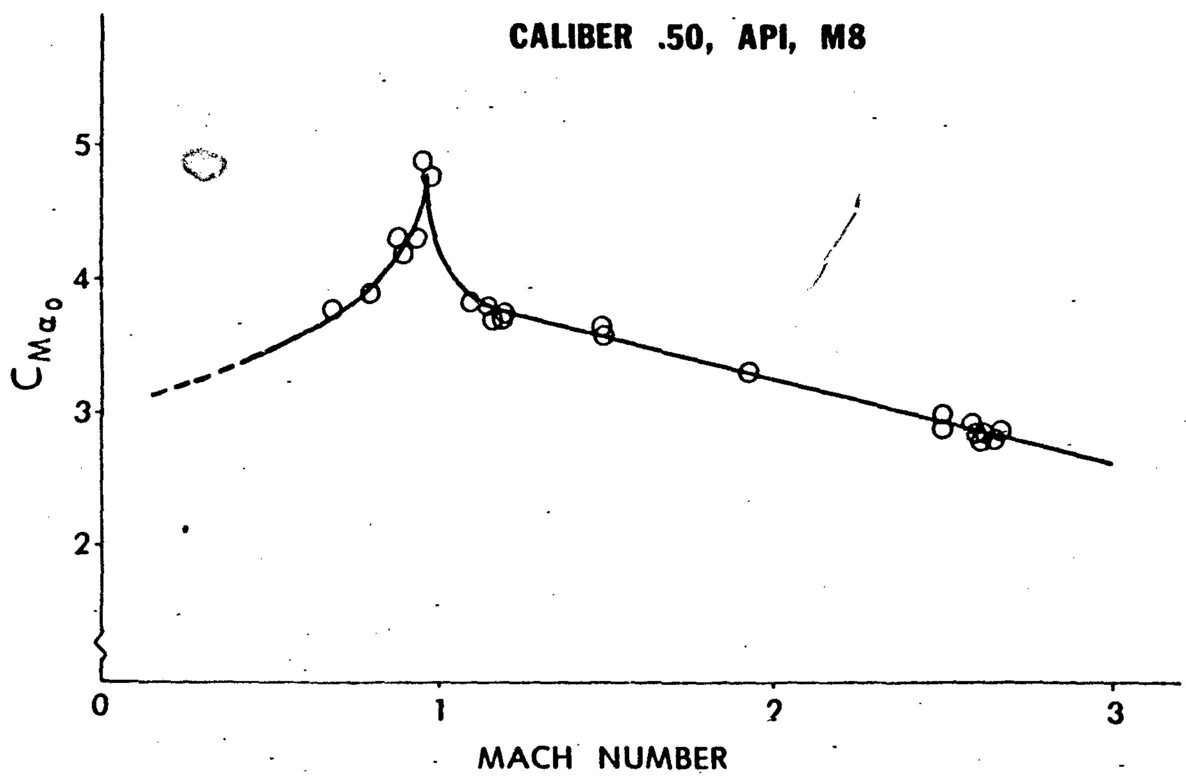

Figure 25. Zero-Yaw Overturning Moment Coefficient versus Mach Number, API, M8.

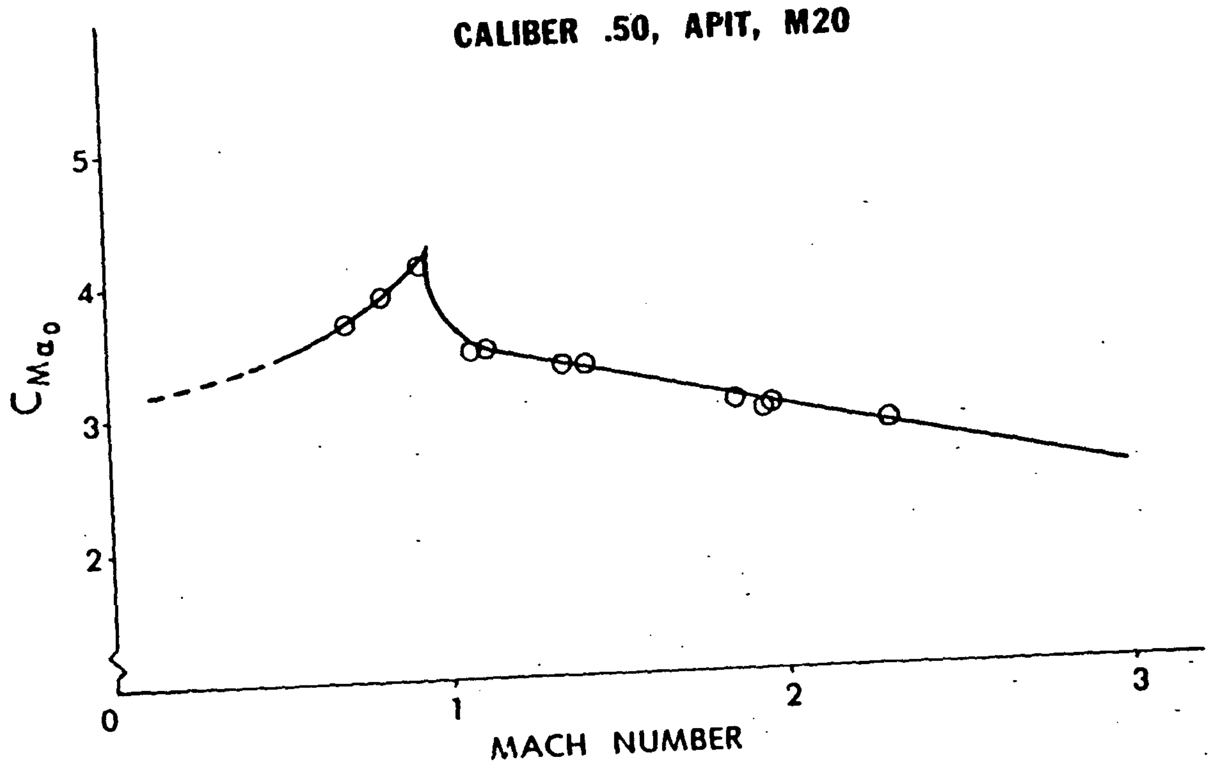

Figure 26. Zero-Yaw Overturning Moment Coefficient versus Mach Number, APIT, M20.

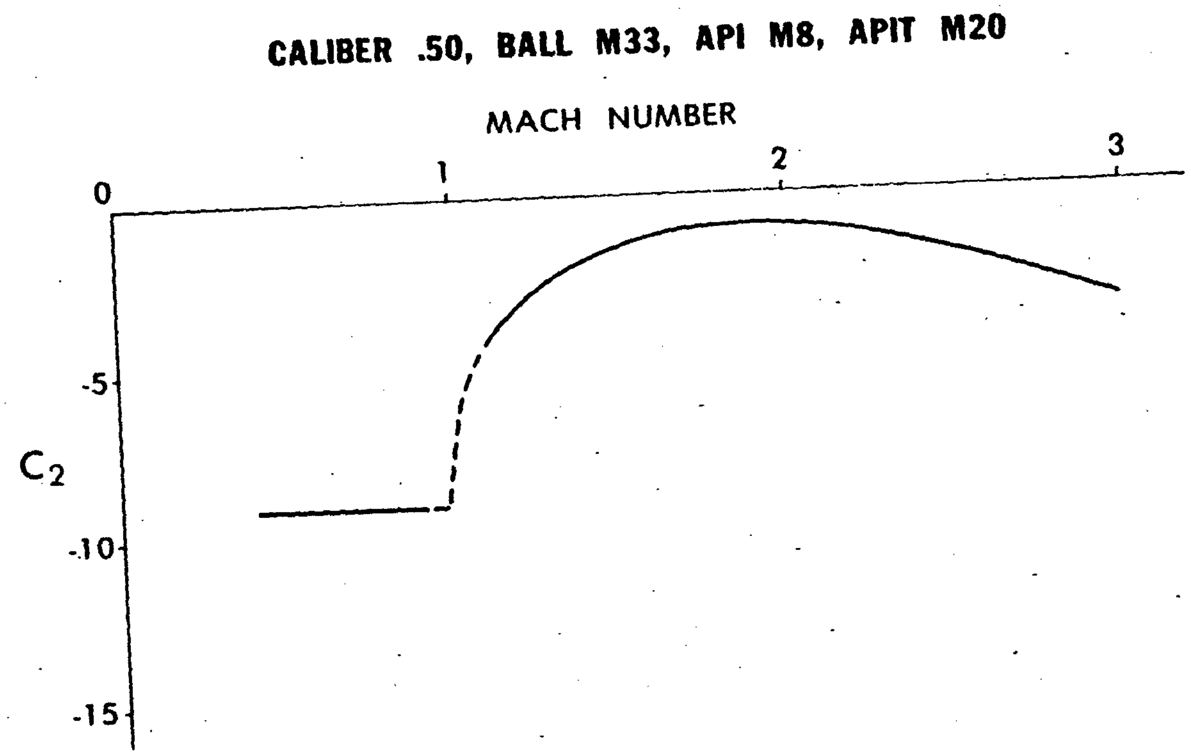

Figure 27. Cubic Overturning Moment Coefficient versus Mach Number.

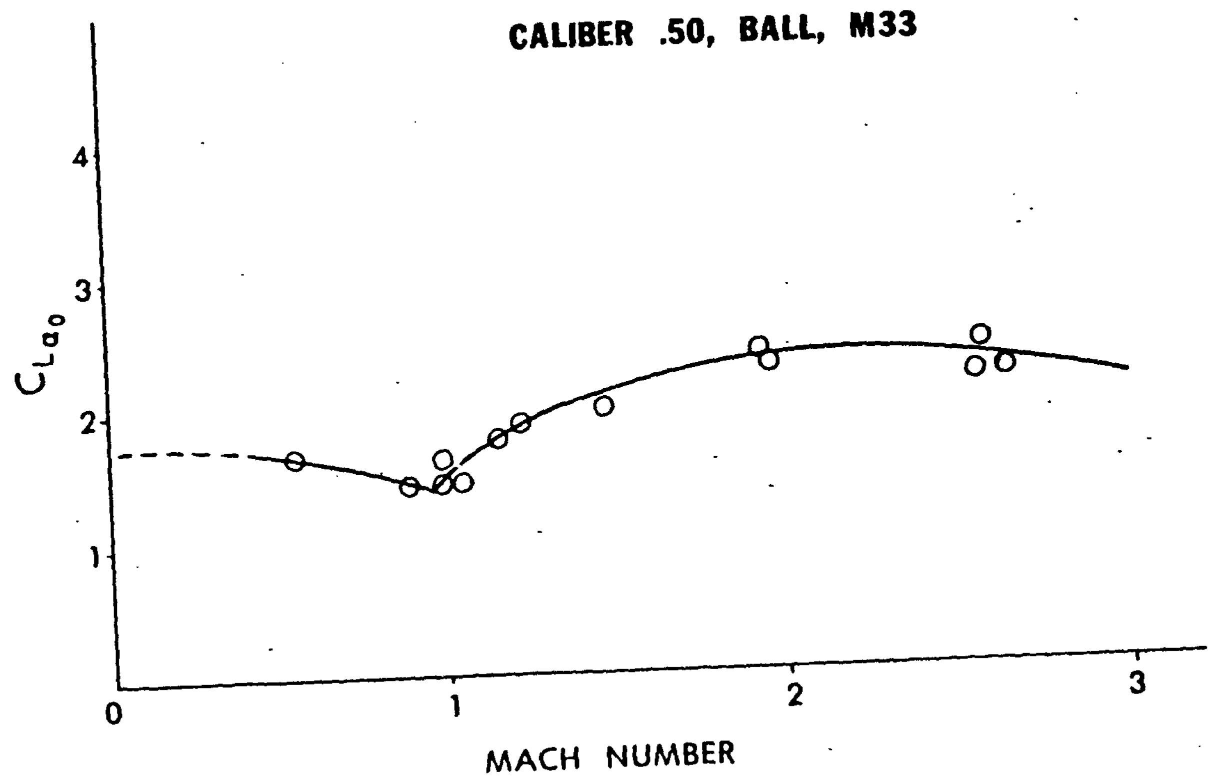

Figure 28. Zero-Yaw Lift Force Coefficient versus Mach Number, Ball, M33

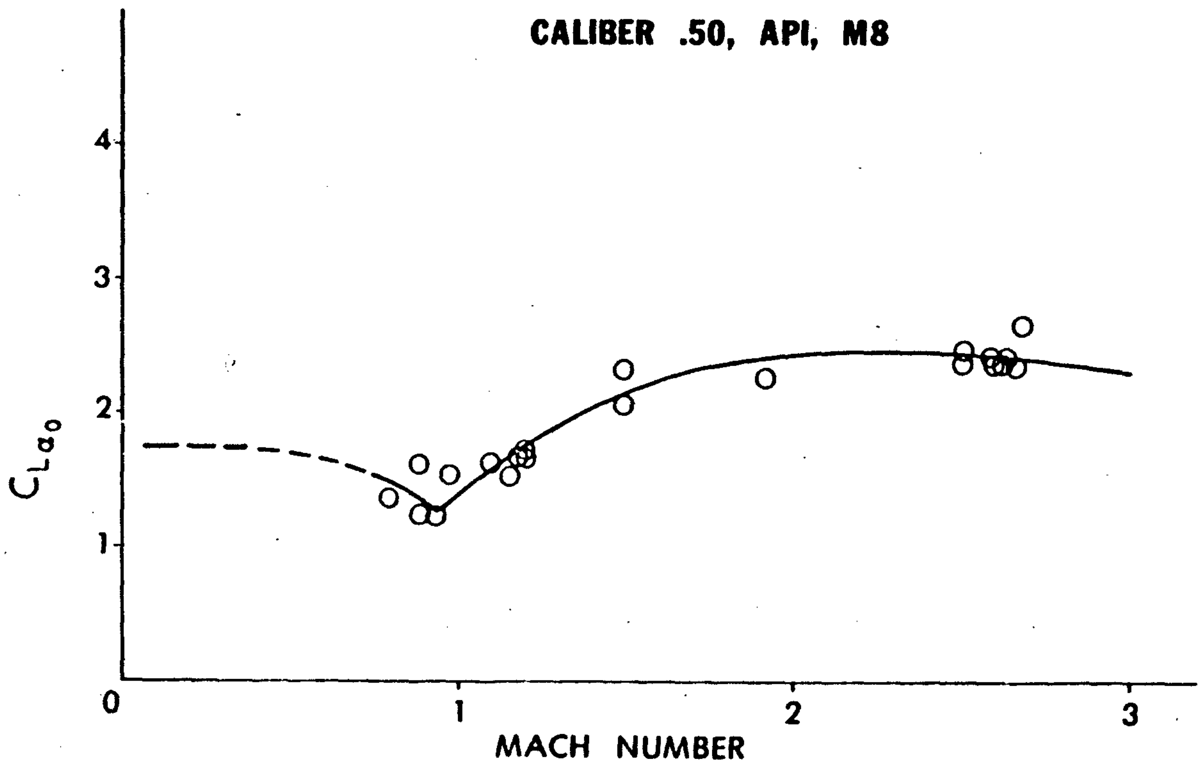

Figure 29. Zero-Yaw Lift Force Coefficient versus Mach Number, API, M8

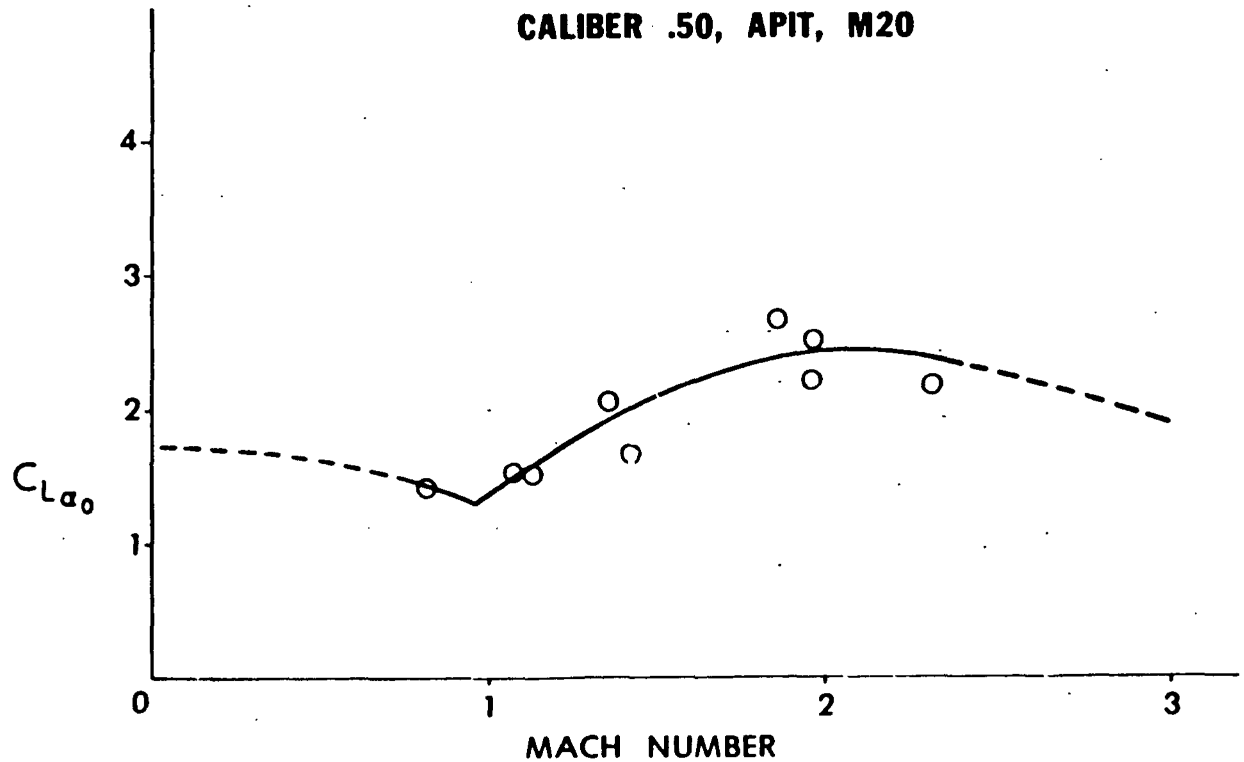

Figure 30. Zero-Yaw Lift Force Coefficient versus Mach Number, APIT, M20.

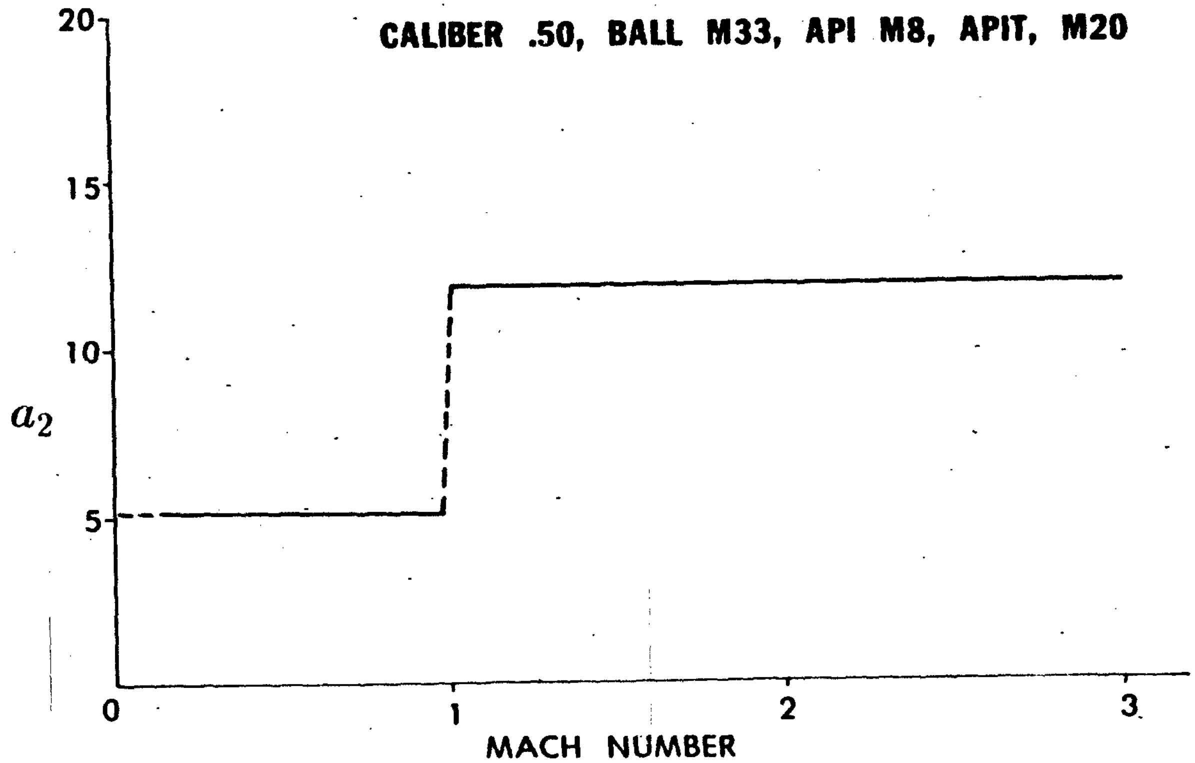

Figure 31. Cubic Lift Force Coefficient versus Mach Number.

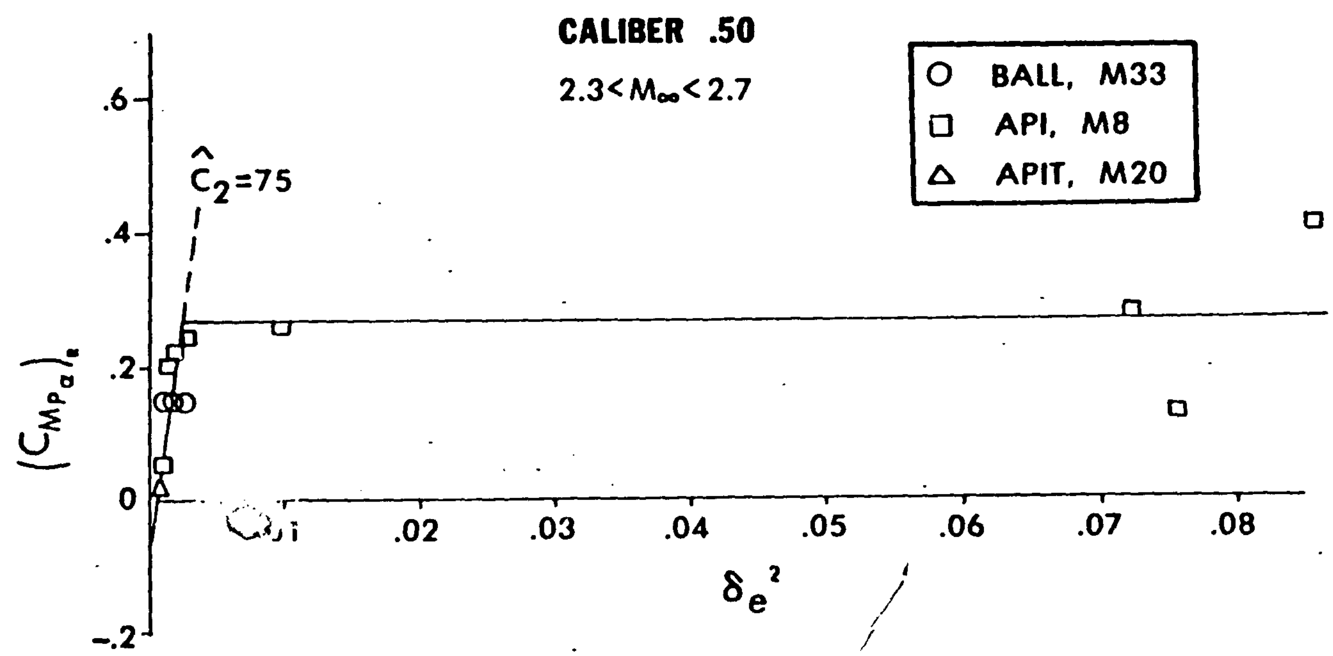

Figure 32. Magnus Moment Coefficient versus Effective Squared Yaw.

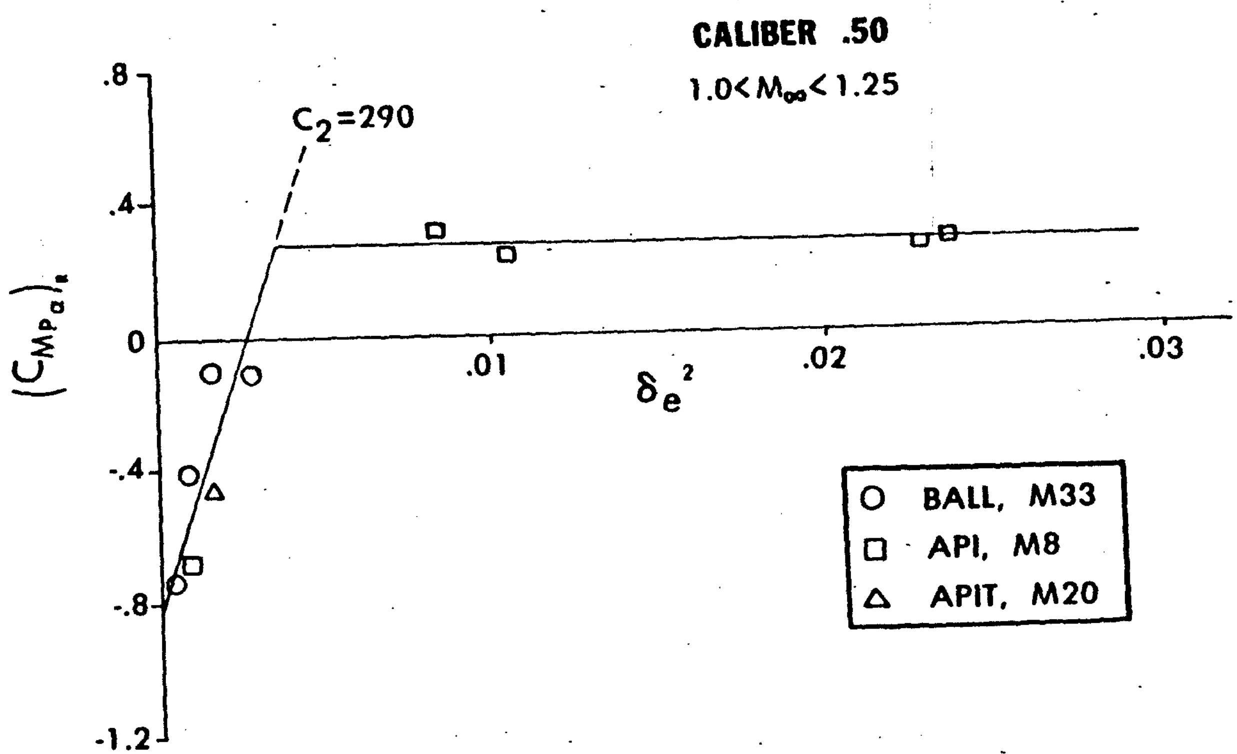

Figure 33. Magnus Moment Coefficient versus Effective Squared Yaw.

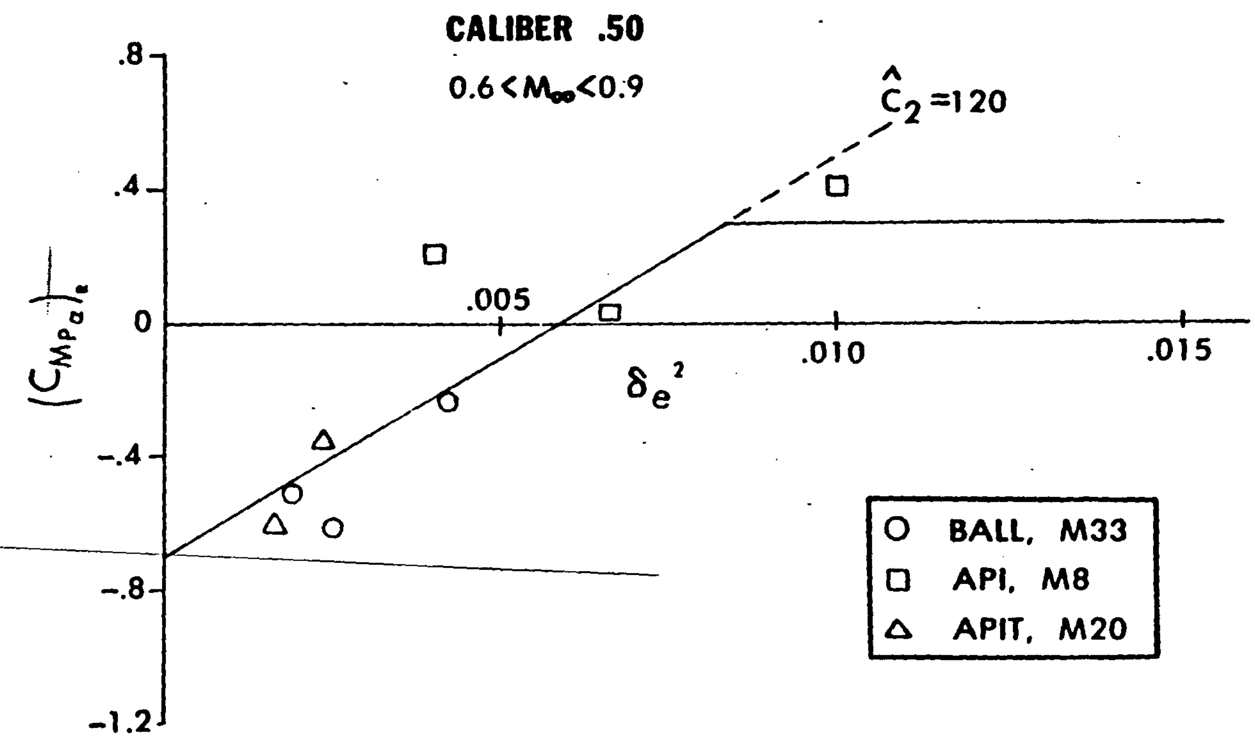

Figure 34. Magnus Moment Coefficient versus Effective Squared Yaw.

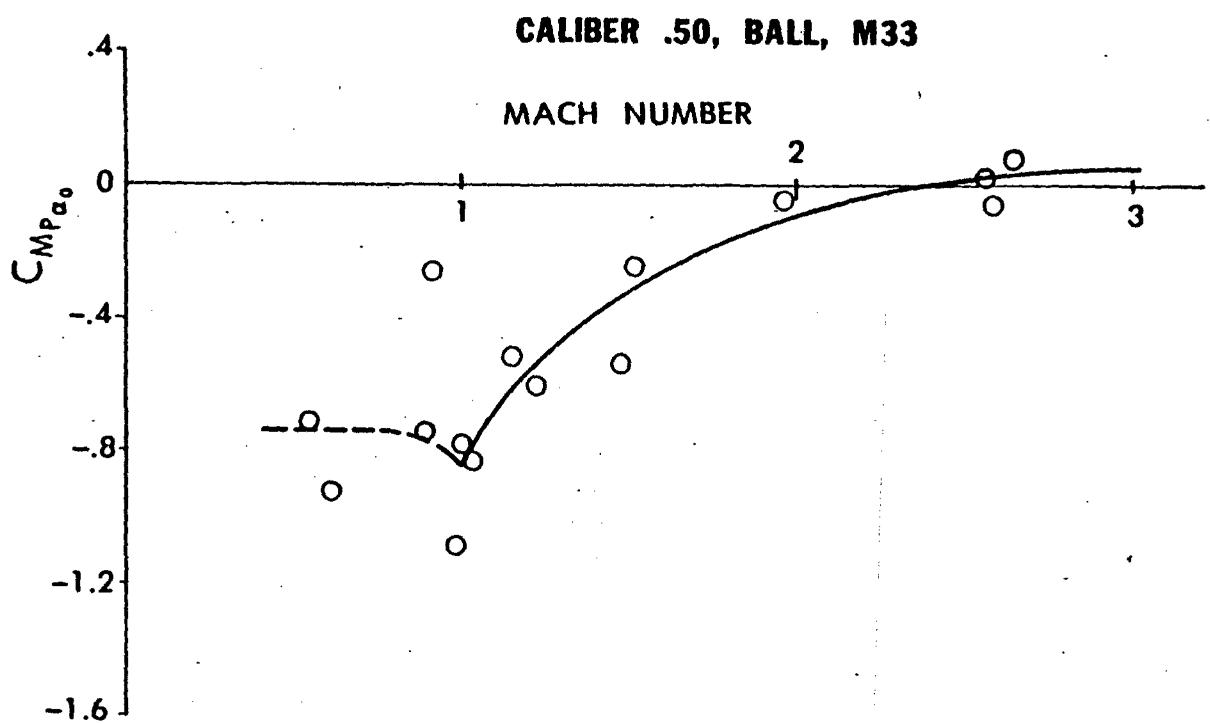

Figure 35. Zero-Yaw Magnus Moment Coefficient versus Mach Number, Ball, M33.

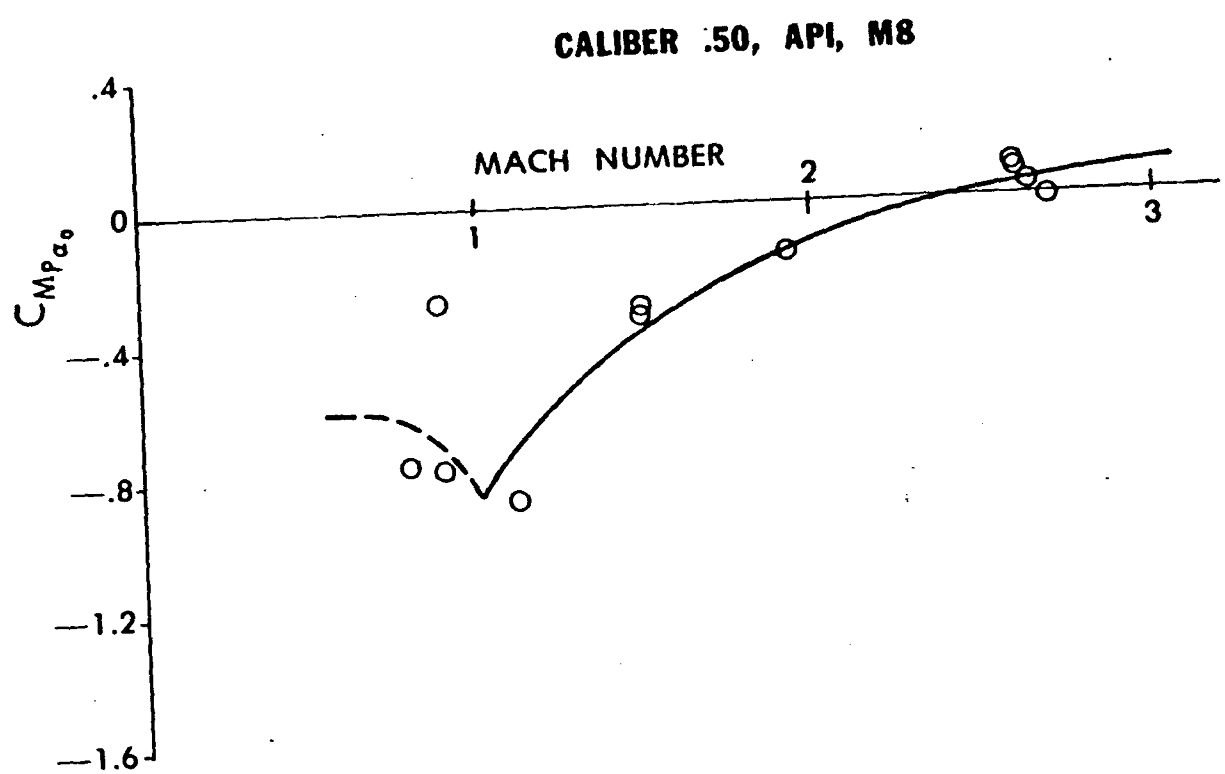

Figure 30. Zero-Yaw Magnus Moment Coefficient versus Mach Number, API, M8.

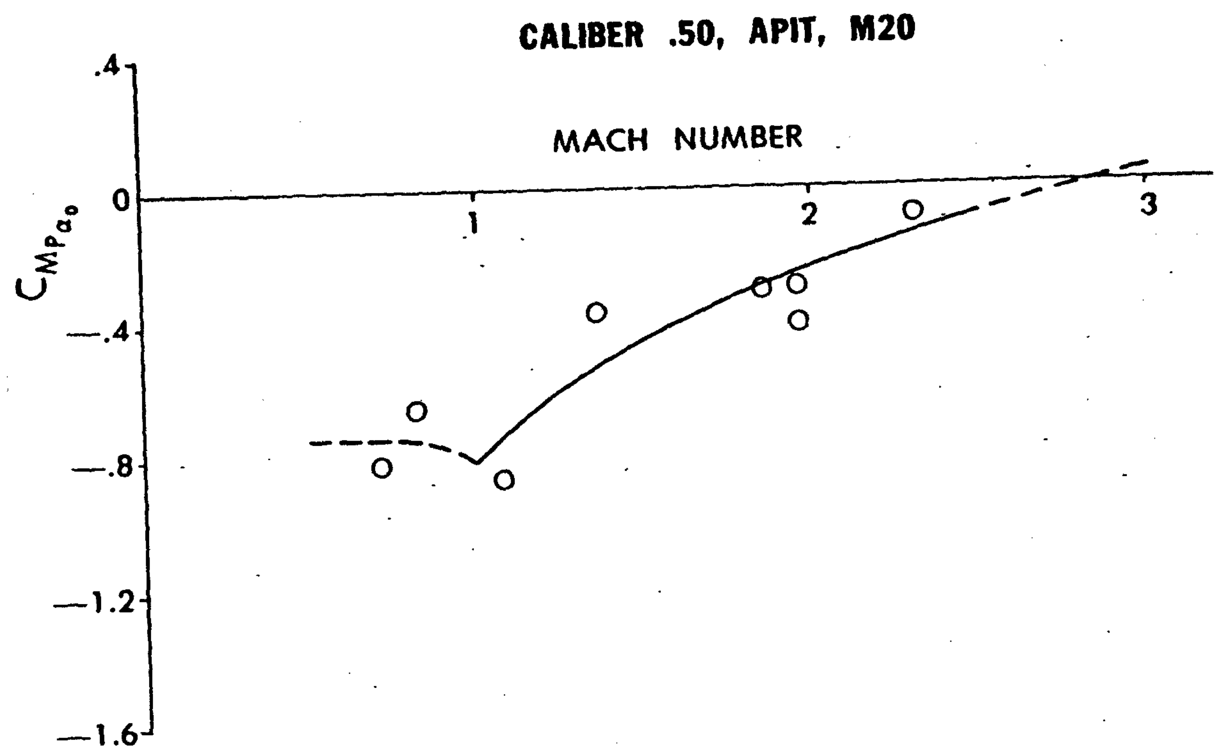

Figure 37. Zero-Yaw Magnus Moment Coefficient versus Mach Number, APIT, M20.

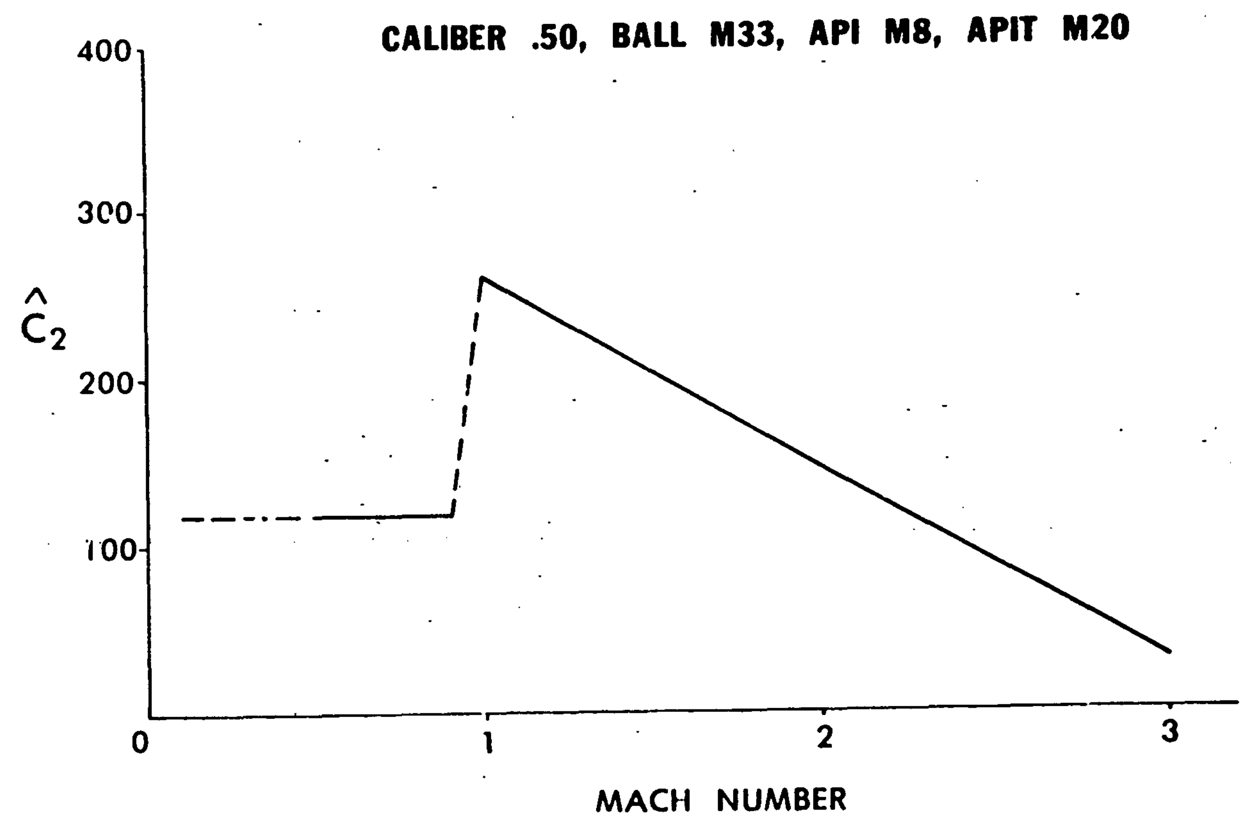

Figure 38. Cubic Magnus Moment Coefficient versus Mach Number.

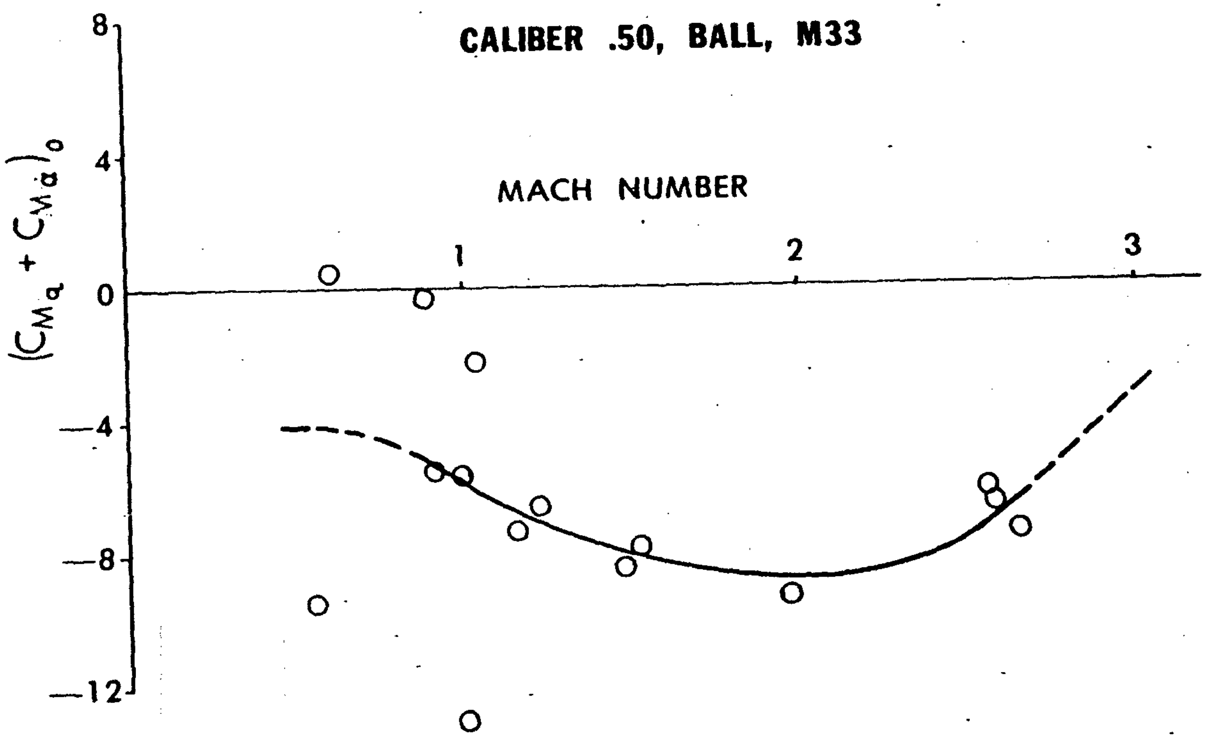

Figure 39. Zero-Yaw Pitch Damping Moment Coefficient versus Mach Number, Ball, M33.

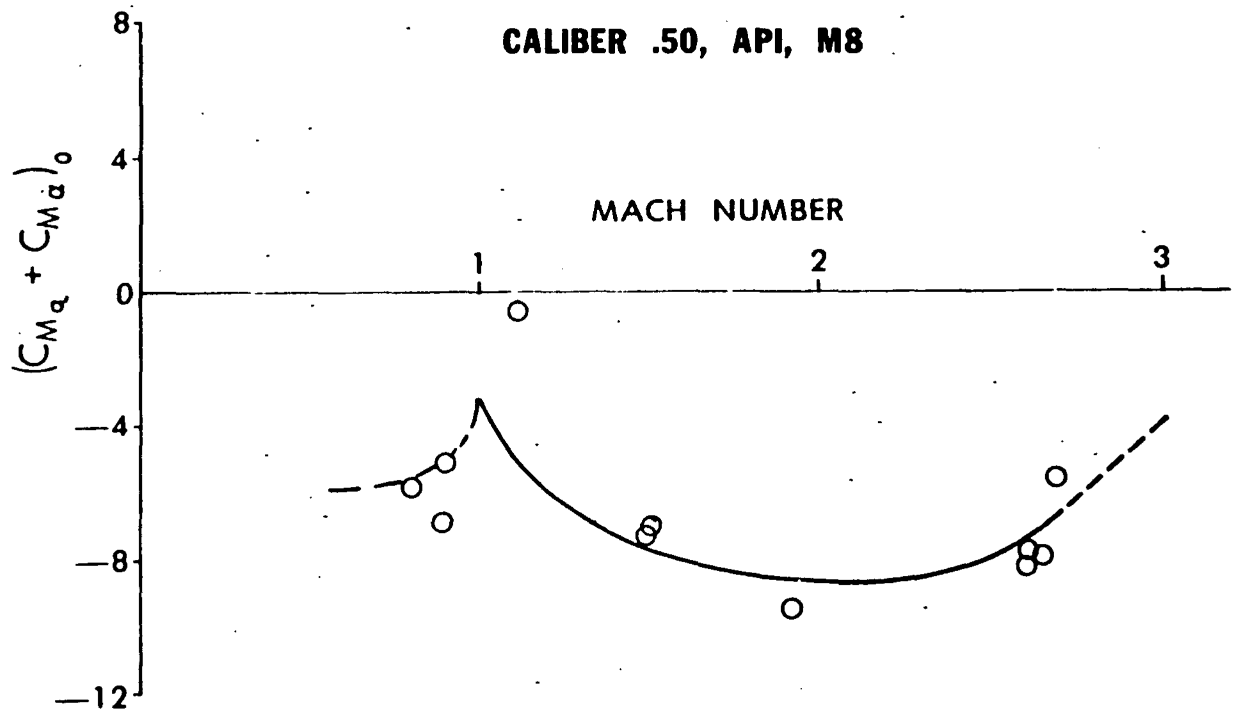

Figure 40. Zero-Yaw Pitch Damping Moment Coefficient versus Mach Number, API, M8.

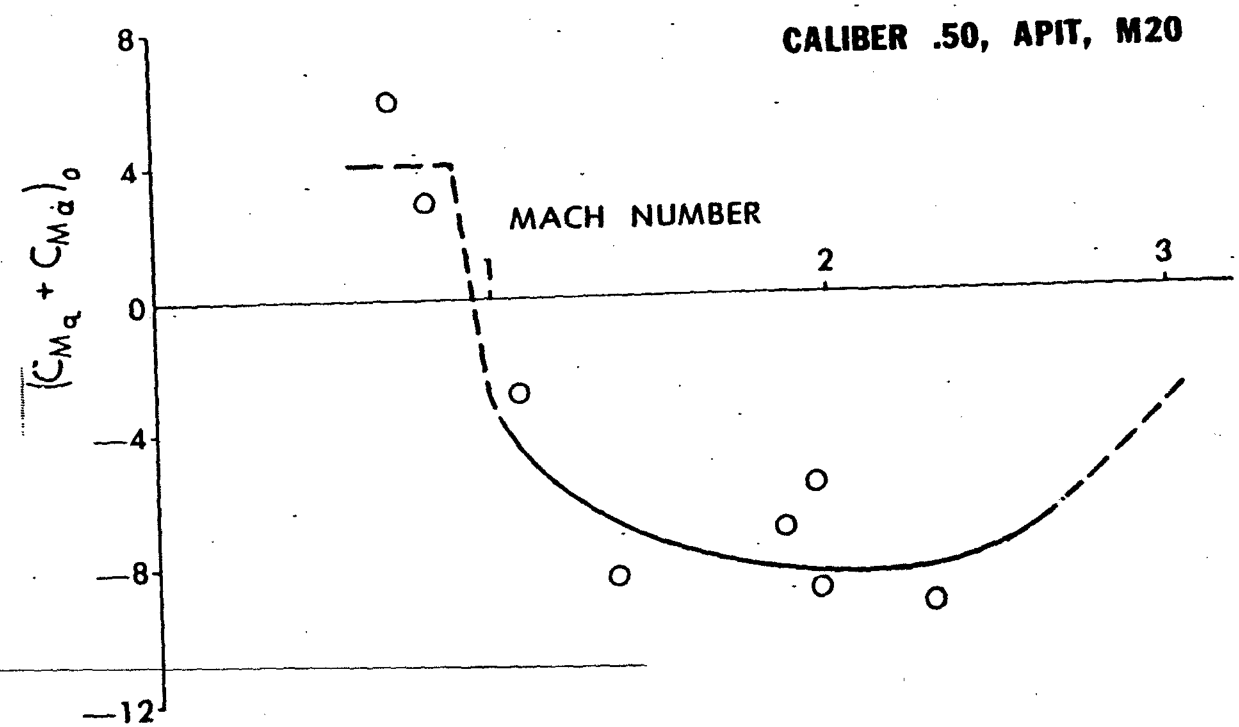

Figure 41. Zero-Yaw Pitch Damping Moment Coefficient versus Mach Number, APIT, M20.

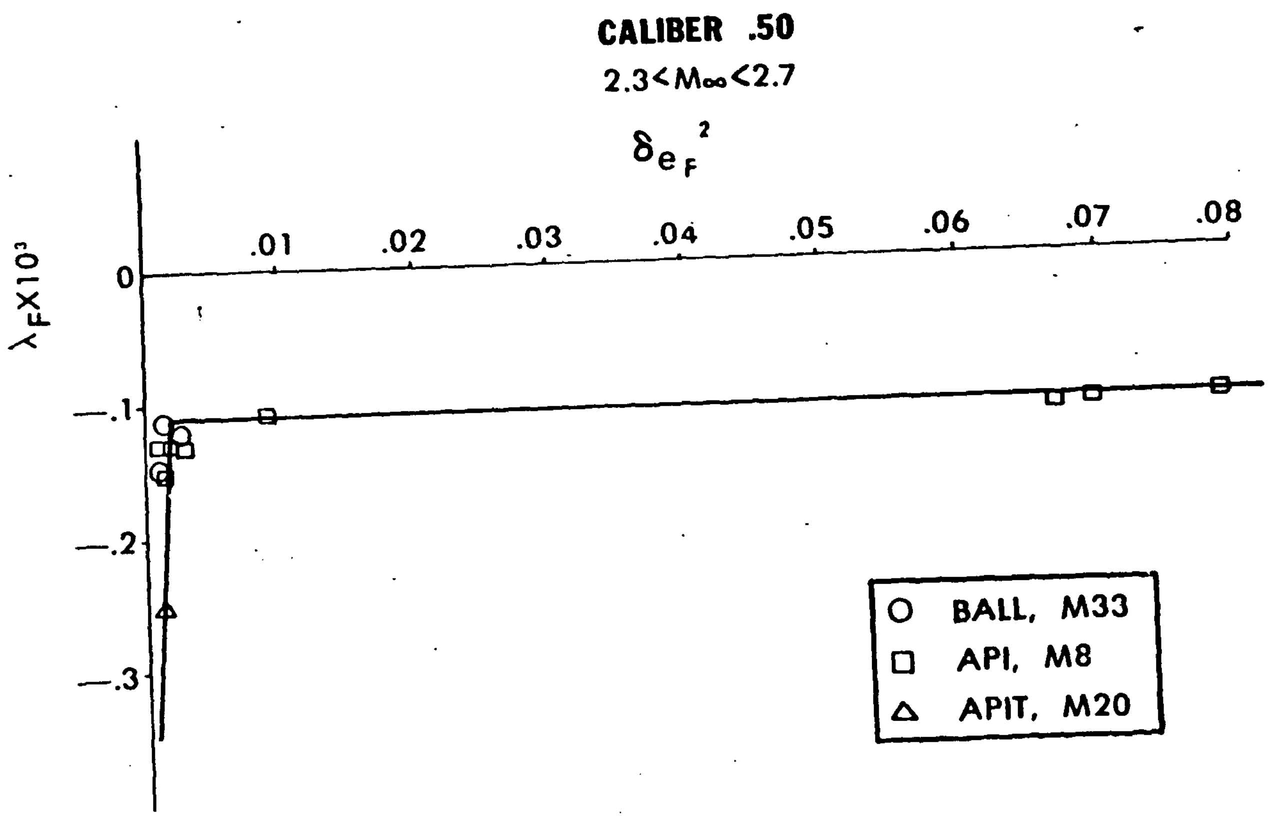

Figure 42. Fast Arm Damping Rate versus Effective Squared Yaw.

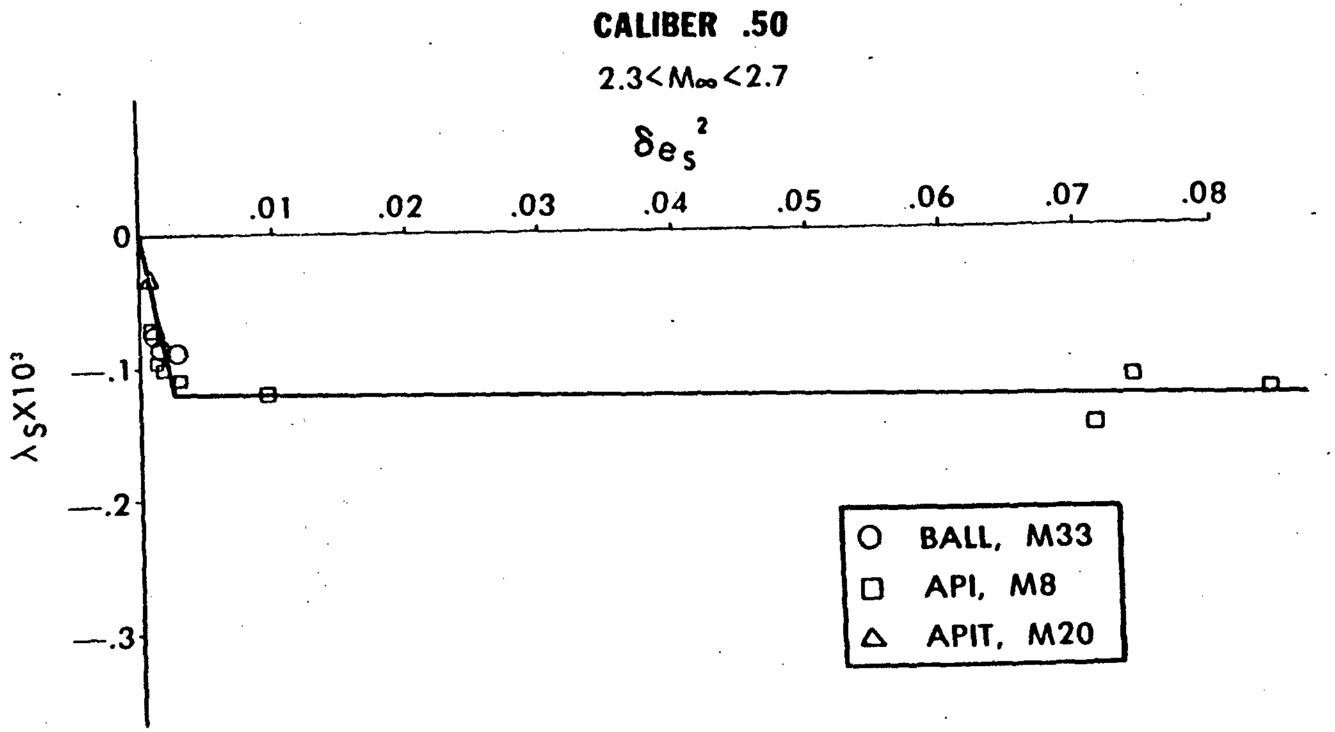

Figure 43. Slow Arm Damping Rate versus Effective Squared Yaw.

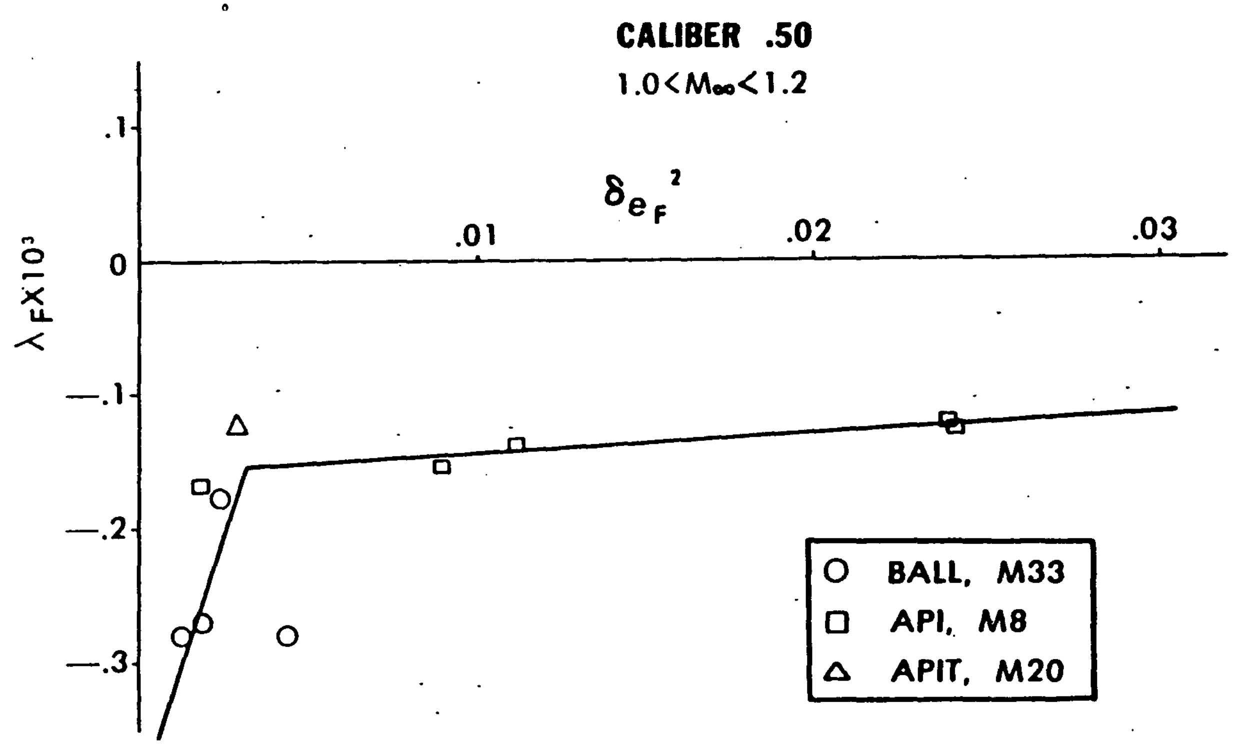

Figure 44. Fast Arm Damping Rate versus Effective Squared Yaw.

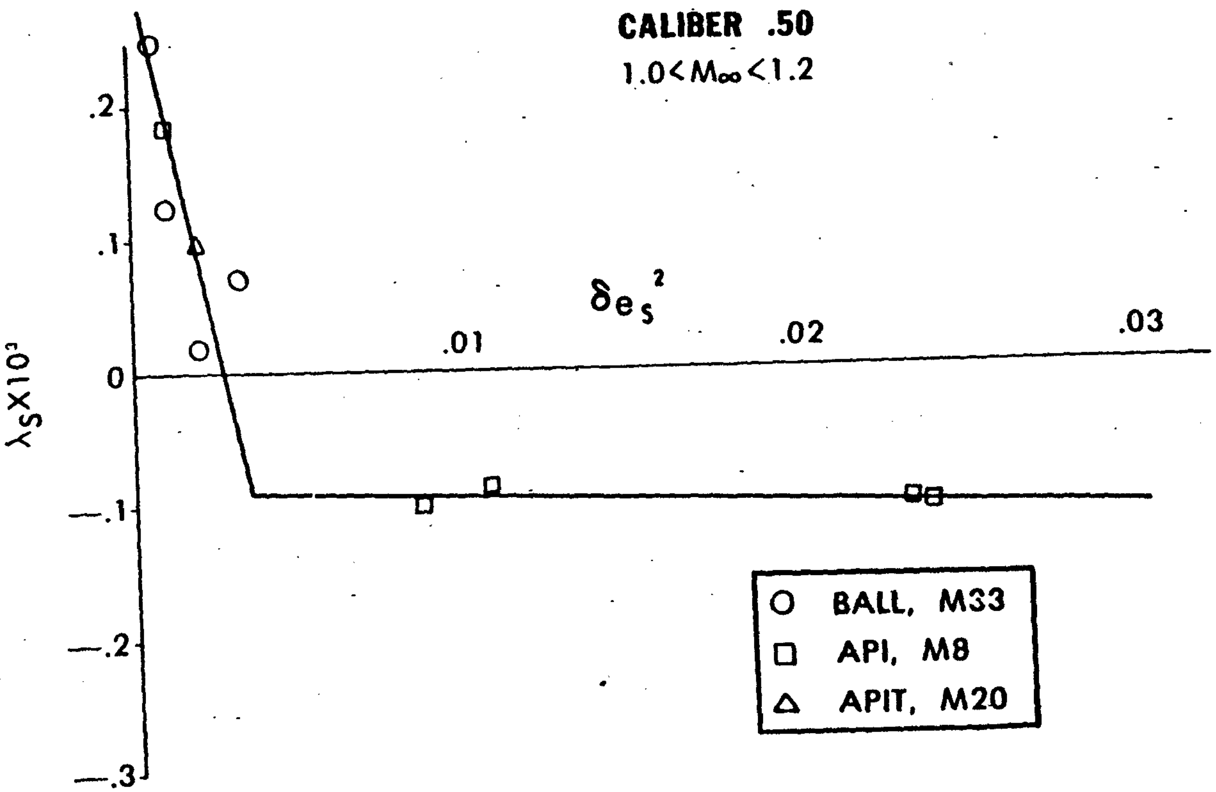

Figure 45. Slow Arm Damping Rate versus Effective Squared Yaw:

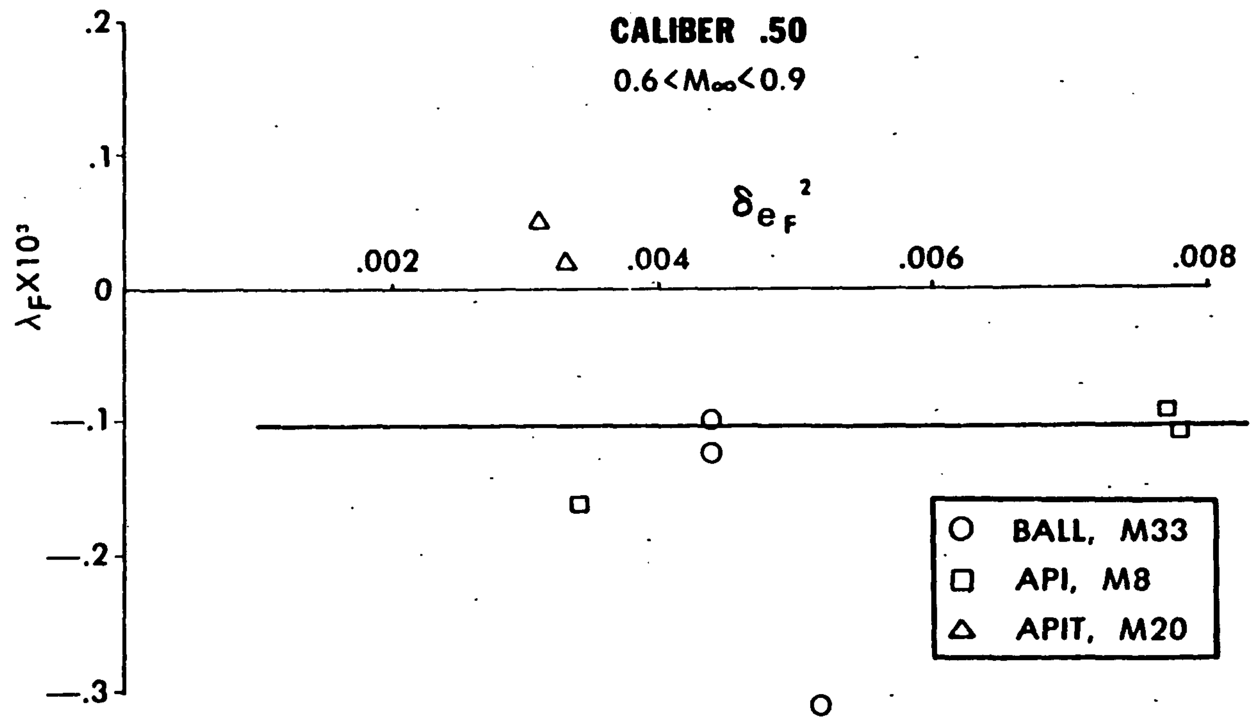

Figure 46. Fast Arm Damping Rate versus Effective Squared Yaw.

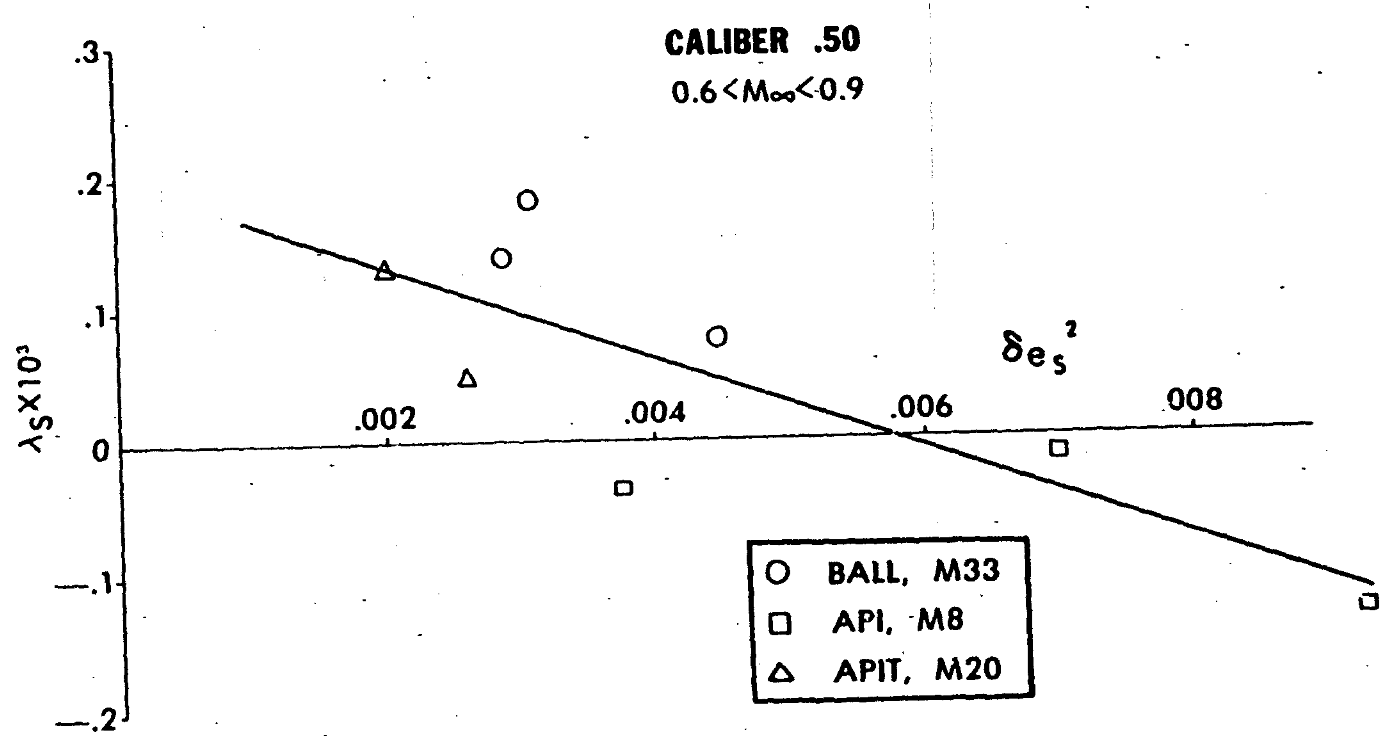

Figure 47. Slow Arm Damping Rate versus Effective Squared Yaw.

Table 1. Average Physical Characteristics of Caliber .50 Projectiles.

Projectile	Reference Diameter (mm)	Weight (grams)	Center of Gravity (cal - base)	Axial Moment of Inertia ($gm\text{-}cm^2$)	Transverse Moment of Inertia ($gm\text{-}cm^2$)
Ball, M33	12.95	42.02	1.78	7.85	74.5
API, M8	12.95	41.98	1.79	7.84	73.9
APIT, M20 (Live Tracer)	12.95	39.77	1.84	7.79	68.5
APIT, M20 (Burnt Tracer)	12.95	38.95	1.88	7.77	66.7

Table 2. Aerodynamic Characteristics of the Ball, M33 Projectile.

Round Number	Mach Number	α_t (degrees)	C_D	C_{M_α}	C_{L_α}	$C_{M_{p\alpha}}$	$(C_{M_q} + C_{M_{\dot\alpha}})$	CP_N (cal - base)
18892	2.653	1.63	.2813	3.01	2.21	.15	-7.4	2.99
18924	2.589	2.54	.2971	3.01	2.41	.15	-6.4	2.90
18891	2.570	1.98	.2923	3.07	2.20	.15	-6.2	3.02
18895	1.972	1.67	.3171	3.40	2.29	.12	-8.8	3.09
18896	1.953	3.54	.3410	3.39	2.43	.20	-8.4	3.01
18899	1.516	1.59	.3489	3.69	--	-.10	-6.6	--
18898	1.475	2.79	.3637	3.70	2.06	.10	-7.1	3.31
18901	1.222	1.84	.3725	3.82	1.89	-.40	-3.9	3.47
18902	1.158	2.26	.3757	3.85	1.79	-.10	-4.6	3.56
18907	1.041	1.59	.3569	4.04	1.46	-.73	0.8	4.01
18908	1.003	2.97	.3461	4.19	1.65	-.10	-7.3	3.88
18906	.989	3.08	.3215	4.24	1.45	-.41	1.0	4.17
18909	.918	3.15	.1505	4.39	--	.74	-12.6	--
18936	.888	2.87	.1372	4.42	1.44	-.52	3.7	4.58
18911	.606	2.87	.1230	3.71	--	-.62	3.0	--
18912	.551	3.30	.1324	3.54	1.67	-.23	-7.9	3.74

Table 3. Aerodynamic Characteristics of the API, M8 Projectile.

Round Number	Mach Number	α_t (degrees)	C_D	C_{M_α}	C_{L_α}	$C_{M_{p\alpha}}$	$(C_{M_q} + C_{M_{\dot\alpha}})$	CP_N (cal - base)
18857	2.686	1.39	.2938	2.88	2.69	.05	-5.5	2.75
18922	2.669	4.62	.3200	2.81	2.48	.26	-7.3	2.79
18856	2.639	2.54	.2991	2.85	2.45	.24	-7.8	2.82
18918	2.628	12.81	.4985	2.65	3.26	.13	-6.2	2.49
18923	2.605	2.08	.2950	2.87	2.38	.22	-7.5	2.86
18920	2.600	1.75	.2956	2.92	2.43	.20	-8.0	2.86
18917	2.511	12.58	.5189	2.76	3.30	.28	-7.9	2.51
18915	2.508	13.57	.5683	2.82	3.40	.41	-7.4	2.50
18859	2.038	.60	.3108	--	--	--	--	--
18860	1.926	1.63	.3260	3.33	2.33	-.02	-8.4	3.04
18866	1.500	1.69	.3507	3.60	2.35	-.14	-5.9	3.12
18867	1.496	1.86	.3525	3.65	2.10	-.07	-6.1	3.28
18929	1.198	7.41	.4542	3.69	1.97	.27	-7.8	3.31
18930	1.197	7.34	.4507	3.67	1.98	.26	-7.5	3.30
18926	1.178	5.00	.4100	3.69	1.79	.24	-7.7	3.46
18875	1.158	4.48	.3984	3.78	1.65	.31	-9.0	3.63
18874	1.109	1.84	.3763	3.84	1.63	-.68	2.7	3.70
18878	.976	2.74	.2388	4.77	1.55	.61	-18.2	4.45
18879	.959	2.55	.1624	4.88	--	.13	-8.2	--
18932	.939	9.63	.2331	4.00	1.50	.02	2.7	4.10
18933	.897	4.39	.1454	4.16	1.30	.41	-8.5	4.67
18935	.892	2.87	.1328	4.28	1.62	.20	-7.7	4.23
18881	.799	4.07	.1407	3.86	1.40	.02	-4.0	4.29
18934	.692	1.75	.1232	3.80	--	--	--	--

Table 4. Aerodynamic Characteristics of the APIT, M20 (Burnt Tracer).

Round Number	Mach Number	$\bar{\alpha}_t$ (degrees)	C_D	C_{M_α}	C_{L_α}	$C_{M_{p\alpha}}$	$(C_{M_q} + C_{M_{\dot{\alpha}}})$	CP_N (cal - base)
13550	2.309	1.59	.3013	2.86	2.23	.01	-8.8	3.02
13551	1.965	1.33	.3250	3.00	2.52	-.33	-8.0	2.94
13552	1.958	1.90	.3261	2.98	2.25	-.11	-4.8	3.04
13549	1.855	1.04	.3182	3.04	2.68	-.25	-6.5	2.90
13553	1.420	1.29	.3589	3.34	1.67	--	--	3.53
13554	1.362	2.13	.3729	3.34	2.10	-.07	-6.3	3.23
13555	1.134	1.78	.3743	3.47	1.54	--	--	3.70
13556	1.075	2.37	.3790	3.47	1.55	-.46	.7	3.68
13557	.941	1.50	.1715	4.11	--	--	--	--
13559	.819	2.55	.1260	3.87	1.45	-.37	4.2	4.34
13560	.748	2.07	.1298	--	--	--	--	--
13561	.710	2.41	.1294	3.66	--	-.62	7.8	--

Table 5. Flight Motion Parameters of the Ball, M33 Projectile.

Round Number	Mach Number	S_g	S_d	$\lambda_F \times 10^3$ (1/cal)	$\lambda_S \times 10^3$ (1/cal)	K_F	K_S	ϕ'_F (r/cal)	ϕ'_S (r/cal)	Spin (r/cal)
18892	2.653	1.81	.8	-.147	-.075	.0191	.0204	.0187	.0037	.213
18924	2.589	1.83	.9	-.120	-.089	.0297	.0318	.0188	.0037	.213
18891	2.570	1.80	.9	-.114	-.084	.0234	.0245	.0187	.0038	.213
18895	1.972	1.61	.6	-.210	-.054	.0177	.0222	.0182	.0043	.214
18896	1.953	1.61	.8	-.165	-.092	.0403	.0445	.0182	.0044	.214
18899	1.516	1.49	.2	-.231	.037	.0132	.0238	.0178	.0048	.214
18898	1.475	1.48	.7	-.173	-.053	.0310	.0361	.0178	.0049	.214
18901	1.222	1.42	-.6	-.271	.126	.0127	.0287	.0174	.0051	.214
18902	1.158	1.42	.3	-.178	.019	.0214	.0327	.0174	.0052	.214
18907	1.041	1.34	-18.1	-.281	.250	.0054	.0257	.0169	.0056	.213
18908	1.003	1.34	.2	-.279	.073	.0263	.0430	.0172	.0057	.217
18906	.989	1.31	-10.0	-.134	.124	.0266	.0458	.0169	.0059	.216
18909	.918	1.18	1.2	-.087	-.232	.0498	.0203	.0153	.0067	.209
18936	.888	1.26	--	-.099	.140	.0209	.0449	.0165	.0062	.215
18911	.606	1.43	--	-.124	.183	.0243	.0434	.0173	.0050	.211
18912	.551	1.47	-.1	-.315	.077	.0352	.0445	.0172	.0048	.209

Table 6. Flight Motion Parameters of the API, M8 Projectile.

Round Number	Mach Number	S_g	S_d	$\lambda_F \times 10^3$ (1/cal)	$\lambda_S \times 10^3$ (1/cal)	K_F	K_S	ϕ'_F (r/cal)	ϕ'_S (r/cal)	Spin (r/cal)
18857	2.686	1.92	.8	-.128	-.071	.0157	.0179	.0191	.0035	.213
18922	2.669	1.93	1.0	-.107	-.121	.0576	.0538	.0191	.0034	.212
18856	2.639	1.93	.9	-.131	-.109	.0308	.0304	.0191	.0035	.212
18918	2.628	2.08	1.0	-.112	-.113	.1626	.1468	.0196	.0032	.214
18923	2.605	1.89	.9	-.129	-.102	.0239	.0263	.0190	.0035	.212
18920	2.600	1.85	.8	-.150	-.096	.0200	.0222	.0188	.0036	.212
18917	2.511	2.04	1.1	-.113	-.148	.1590	.1442	.0197	.0033	.217
18915	2.508	1.99	1.4	-.108	-.124	.1729	.1564	.0196	0034	.217
18859	2.038	--	--	--	--	.0038	.0095	--	--	--
18860	1.926	1.67	.4	-.244	-.007	.0136	.0244	.0185	.0042	.213
18866	1.500	1.50	.3	-.215	.018	.0156	.0243	.0178	.0047	.212
18867	1.496	1.49	.4	-.201	.003	.0181	.0261	.0178	.0048	.213
18929	1.198	1.55	.9	-.126	-.105	.0882	.0902	.0183	.0047	.217
18930	1.197	1.54	.9	-.124	-.103	.0863	.0907	.0183	.0047	.216
18926	1.178	1.50	.9	-.138	-.088	.0576	.0629	.0179	.0048	.214
18875	1.158	1.45	.9	-.153	-.101	.0517	.0559	.0177	.0050	.214
18874	1.109	1.42	--	-.168	.184	.0108	.0294	.0175	.0051	.213
18878	.976	1.20	.7	-.352	-.037	.0219	.0404	.0162	.0069	.218
18879	.959	1.07	.5	-.318	.063	.0192	.0389	.0140	.0082	.209
18932	.939	1.33	--	.119	-.115	.1499	.0703	.0166	.0056	.209
18933	.897	1.29	1.1	-.094	-.134	.0595	.0457	.0164	.0059	.210
18935	.892	1.24	.8	-.163	-.038	.0370	.0318	.0159	.0062	.209
18881	.799	1.39	.6	-.110	-.015	.0454	.0537	.0171	.0053	.211
18934	.692	1.44	--	--	--	.0079	.0277	.0175	.0050	.212

Table 7. Flight Motion Parameters of the APIT, M20 Projectile (Burnt Tracer).

Round Number	Mach Number	S_g	S_d	$\lambda_F \times 10^3$ (1/cal)	$\lambda_S \times 10^3$ (1/cal)	K_F	K_S	ϕ'_F (r/cal)	ϕ'_S (r/cal)	Spin (r/cal)
13550	2.309	2.09	.4	-.252	-.033	.0139	.0226	.0213	.0034	.213
13551	1.965	2.02	-.1	-.330	.062	.0066	.0210	.0213	.0036	.214
13552	1.958	2.01	.4	-.174	-.015	.0168	.0272	.0212	.0036	.213
13549	1.855	1.94	.1	-.270	.024	.0073	.0156	.0208	.0037	.211
13553	1.420	1.83	-1.1	-.351	.172	.0039	.0205	.0207	.0040	.213
13554	1.362	1.81	.4	-.210	-.012	.0168	.0315	.0208	.0041	.214
13555	1.134	1.74	--	--	--	.0044	.0278	.0206	.0043	.214
13556	1.075	1.75	-5.9	-.124	.096	.0166	.0365	.0207	.0043	.215
13557	.941	1.36	--	--	--	.0241	.0049	.0182	.0058	.206
13559	.819	1.48	--	.019	.048	.0254	.0362	.0190	.0052	.209
13560	.748	--	--	--	--	.0037	.0335	--	--	--
13561	.710	1.57	--	.050	.130	.0179	.0372	.0195	.0049	.209

Table 8. Tracer-On Drag Measurements for the APIT, M20 Projectile.

Round Number	Mach Number	α_t (degrees)	$C_{D_{(R)}}$	C_{D_0}
30461	2.502	.31	.2748	.274
30460	2.497	.27	.2656	.265
30467	2.478	.63	.2741	.274
17089	2.430	*	.2759	.275
30462	1.882	.59	.3029	.302
17159	1.533	*	.3254	.325
17158	1.528	*	.3293	.329
17160	1.525	*	.3193	.319
30475(a)	1.015	1.79	.3081	.304
30474(a)	1.007	1.00	.3028	.302
30474(b)	.983	1.05	.2263	.225
30475(b)	.973	2.30	.1596	.152
30474(c)	.967	1.63	.1603	.158
30473	.966	1.28	.1439	.142

Notes: * Very small yaw (α_t < .5 degree)
( ) Denotes split reduction

References

1. Hitchcock, H.P., "Aerodynamic Data for Spinning Projectiles," US Army Ballistic Research Laboratory, Aberdeen Proving Ground, Maryland, BRL Report No. 620, October 1947. (AD 800469)

2. Braun, W.F., "The Free Flight Aerodynamics Range," US Army Ballistic Research Laboratory, Aberdeen Proving Ground, Maryland, BRL Report No. 1048, August 1958. (AD 202249)

3. Rogers, W.K., "The Transonic Free Flight Range," US Army Ballistic Research Laboratory, Aberdeen Proving Ground, Maryland, BRL Report No. 1044, June 1958. (AD 200177)

4. Murphy C.H., "Data Reduction for the Free Flight Spark Ranges," US Army Ballistic Research Laboratory, Aberdeen Proving Ground, Maryland, BRL Report No. 900, February 1954. (AD 35833)

5. Murphy, C.H., "The Measurement of Non-Linear Forces and Moments by Means of Free Flight Tests," US Army Ballistic Research Laboratory, Aberdeen Proving Ground, Maryland, BRL Report No. 974, February 1956. (AD 93521)

6. Murphy, C.H, "Free Flight Motion of Symmetric Missiles," US Army Ballistic Research Laboratory, Aberdeen Proving Ground, Maryland, BRL Report No. 1216, July 1963. (AD 442757)

INTENTIONALLY LEFT BLANK.

List of Symbols

a_2	=	cubic lift force coefficient	
C_2	=	cubic static moment coefficient	
$\hat{C}_2$	=	cubic Magnus moment coefficient	
C_D	=	$\frac{\text{Drag Force}}{[(1/2)\rho V^2 S]}$	
C_{D0}	=	zero-yaw drag coefficient	
$C_{D_{\delta^2}}$	=	quadratic yaw drag coefficient	
C_{L_α}	=	$\frac{\text{Lift Force}}{[(1/2)\rho V^2 S \delta]}$	Positive coefficient: Force in plane of total angle of attack, α_t, $\perp$ to trajectory in direction of α_t. (α_t directed from trajectory to missile axis.) $\delta = \sin\alpha_t$.
C_{N_α}	=	$\frac{\text{Normal Force}}{[(1/2)\rho V^2 S \delta]}$	Positive coefficient: Force in plane of total angle of attack, α_t, $\perp$ to missile axis in direction of α_t. $C_{N_\alpha} \cong C_{L_\alpha} + C_D$
C_{M_α}	=	$\frac{\text{Static Moment}}{[(1/2)\rho V^2 S d \delta]}$	Positive coefficient: Moment increases angle of attack α_t.
$C_{M_{p\alpha}}$	=	$\frac{\text{Magnus Moment}}{[(1/2)\rho V^2 S d (pd/V) \delta]}$	Positive coefficient: Moment rotates nose $\perp$ to plane of α_t in direction of spin.
$C_{N_{p\alpha}}$	=	$\frac{\text{Magnus Force}}{[(1/2)\rho V^2 S (pd/V) \delta]}$	Negative coefficient: Force acts in direction of 90° rotation of the positive lift force against spin.

List of Symbols (Continued)

For most exterior ballistic uses, where $\dot{\alpha} \approx q$, $\dot{\beta} \approx -r$, the definition of the damping moment sum is equivalent to:

$(C_{M_q} + C_{M_{\dot{\alpha}}})$	=	$\frac{\text{Damping Moment}}{[(1/2)\rho V^2 S d\,(q_t d/V)]}$	Positive coefficient: Moment increases angular velocity.
C_{l_p}	=	$\frac{\text{Roll Damping Moment}}{[(1/2)\rho V^2 S d\,(p d/V)]}$	Negative coefficient: Moment decreases rotational velocity.
C_{P_N}	=	center of pressure of the normal force, positive from base to nose	
α, β	=	angle of attack, side slip	
α_t	=	$(\alpha^2 + \beta^2)^{\frac{1}{2}} = \sin^{-1}\delta$, total angle of attack	
λ_F	=	fast mode damping rate	negative λ indicates damping
λ_S	=	slow mode damping rate	negative λ indicates damping
ρ	=	air density	
ϕ'_F	=	fast mode frequency	
ϕ'_S	=	slow mode frequency	
$c.m.$	=	center of mass	
d	=	body diameter of projectile, reference length	
d_2	=	cubic pitch damping moment coefficient	
I_x	=	axial moment of inertia	

List of Symbols (Continued)

I_y	=	transverse moment of inertia
K_F	=	magnitude of the fast yaw mode
K_S	=	magnitude of the slow yaw mode
l	=	length of projectile
m	=	mass of projectile
M	=	Mach number
p	=	roll rate
q, r	=	transverse angular velocities
q_t	=	$(q^2 + r^2)^{\frac{1}{2}}$
R	=	subscript denotes range value
s	=	dimensionless arc length along the trajectory
S	=	$(\pi d^2/4)$, reference area
S_d	=	dynamic stability factor
S_g	=	gyroscopic stability factor
V	=	velocity of projectile

List of Symbols (Continued)

<u>Effective Squared Yaw Parameters</u>

$\bar{\delta}$	$\cong$	$K_F^2 + K_S^2$
δ_e^2	$=$	$K_F^2 + K_S^2 + \dfrac{(\phi'_F K_F^2 - \phi'_S K_S^2)}{(\phi'_F - \phi'_S)}$
$\delta_{e_F}^2$	$=$	$K_F^2 + 2 K_S^2$
$\delta_{e_S}^2$	$=$	$2 K_F^2 + K_S^2$
$\delta_{e_{HH}}^2$	$=$	$\left(\dfrac{I_y}{I_x}\right)\left[\dfrac{(\phi'_F + \phi'_S)(K_S^2 - K_F^2)}{(\phi'_F - \phi'_S)}\right]$
$\delta_{e_{TH}}^2$	$=$	$\left(\dfrac{I_x}{I_y}\right)\left[\dfrac{(K_F^2 \phi_F'^2 - K_S^2 \phi_S'^2)}{(\phi_F'^2 - \phi_S'^2)}\right]$
$\delta_{e_{HT}}^2$	$=$	$\dfrac{(\phi'_F K_S^2 - \phi'_S K_F^2)}{(\phi'_F - \phi'_S)}$

No of Copies	Organization
(...lass., unlimited) 12 (...lass., limited) 2 (...mited) 2	Administrator Defense Technical Info Center ATTN: DTIC-DDA Cameron Station Alexandria, VA 22304-6145
1	HQDA (SARD-TR) WASH DC 20310-0001
1	Commander US Army Materiel Command ATTN: AMCDRA-ST 5001 Eisenhower Avenue Alexandria, VA 22333-0001
1	Commander US Army Laboratory Command ATTN: AMSLC-DL Adelphi, MD 20783-1145
2	Commander Armament RD&E Center US Army AMCCOM ATTN: SMCAR-MSI Picatinny Arsenal, NJ 07806-5000
2	Commander Armament RD&E Center US Army AMCCOM ATTN: SMCAR-TDC Picatinny Arsenal, NJ 07806-5000
1	Director Benet Weapons Laboratory Armament RD&E Center US Army AMCCOM ATTN: SMCAR-CCB-TL Watervliet, NY 12189-4050
1	Commander US Army Armament, Munitions and Chemical Command ATTN: SMCAR-ESP-L Rock Island, IL 61299-5000
1	Commander US Army Aviation Systems Command ATTN: AMSAV-DACL 4300 Goodfellow Blvd. St. Louis, MO 63120-1798
1	Director US Army Aviation Research and Technology Activity Ames Research Center Moffett Field, CA 94035-1099

No of Copies	Organization
1	Commander US Army Missile Command ATTN: AMSMI-RD-CS-R (DOC) Redstone Arsenal, AL 35898-5010
1	Commander US Army Tank-Automotive Command ATTN: AMSTA-TSL (Technical Library) Warren, MI 48397-5000
1	Director US Army TRADOC Analysis Command ATTN: ATAA-SL White Sands Missile Range, NM 88002-5502
(Class. only) 1	Commandant US Army Infantry School ATTN: ATSH-CD (Security Mgr.) Fort Benning, GA 31905-5660
(Unclass. only) 1	Commandant US Army Infantry School ATTN: ATSH-CD-CSO-OR Fort Benning, GA 31905-5660
(Class. only) 1	The Rand Corporation P.O. Box 2138 Santa Monica, CA 90401-2138
1	Air Force Armament Laboratory ATTN: AFATL/DLODL Eglin AFB, FL 32542-5000

<u>Aberdeen Proving Ground</u>

Dir, USAMSAA
    ATTN: AMXSY-D
        AMXSY-MP, H. Cohen
Cdr, USATECOM
    ATTN: AMSTE-TO-F
Cdr, CRDEC, AMCCOM
    ATTN: SMCCR-RSP-A
        SMCCR-MU
        SMCCR-MSI
Dir, VLAMO
    ATTN: AMSLC-VL-D

No. of Copies	Organization
2	Air Force Armament Laboratory ATTN: AFATL/FXA Mr. G. Abate Mr. G. Winchenbach Eglin AFB, FL 32542-5000
1	Director Requirements and Programs Directorate HQ, TRADOC Analysis Command ATTN: ATRC-RP Fort Leavenworth, KS 66027-5200
1	Commander TRADOC Analysis Command ATTN: ATRC Fort Leavenworth, KS 66027-5200
1	Director TRADOC Analysis Command - White Sands Missile Range White Sands Missile Range, NM 88002-5502
1	US Army JFK Center ATTN: ATSU-CD-ML Mr. S. Putnam Fort Bragg, NC 28307-5007
1	Commander US Army Materiel Command ATTN: AMXSO Mr. J. McKernan 5001 Eisenhower Avenue Alexandria, VA 22333-0001
1	President US Army Infantry Board ATTN: ATZB-IB-SA Mr. L. Tomlinson Fort Benning, GA 31905-5800
1	Commander Naval Sea Systems Command ATTN: Code 62CE Mr. R. Brown Washington, DC 20362-5101
4	Commanding Officer Naval Weapons Support Center ATTN: Code 2021, Bldg. 2521 Mr. C. Zeller ATTN: Code 2022 Mr. R. Henry Mr. G. Dornick Mr. J. Maassen Crane, IN 47522-5020

No. of Copies	Organization
19	Commander Armament RD&E Center US Army AMCCOM ATTN: SMCAR-SCJ Mr. J. Ackley Mr. V. Shisler Mr. H. Wreden Mr. J. Hill ATTN: SMCAR-CCL-AD Mr. F. Puzycki Mr. W. Schupp Mr. R. Mazeski Mr. D. Conway ATTN: SMCAR-CCL-FA Mr. R. Schlenner Mr. J. Fedewitz Mr. P. Wyluda ATTN: SMCAR-SCA-AP Mr. W. Bunting Mr. P. Errante ATTN: SMCAR-AET-AP Mr. R. Kline Mr. Chiu Ng Mr. H. Hudgins Mr. S. Kahn ATTN: SMCAR-FSF-GD Mr. K. Pfleger ATTN: SMCAR-CCL-CF Mr. J. Cline Picatinny Arsenal, NJ 07806-5000
1	Commanding General MCDEC ATTN: Code D091 Fire Power Division Quantico, VA 22134-5080
1	US Secret Service J.J. Rowley Training Center ATTN: Mr. B. Seiler 9200 Powder Mill Road, RD 2 Laurel, MD 20707
1	Commander Naval Surface Warfare Center ATTN: Code G31 Mr. F. Willis Dahlgren, VA 22408-5000
1	Tioga Engineering Company ATTN: Mr. W. Davis, Jr. 13 Cone Street Wellsboro, PA 16901

Aberdeen Proving Ground

Director, USAMSAA
  ATTN: AMXSY-J
    Mr. K. Jones
    Mr. M. Carroll
    Mr. J. Weaver
    Mr. E. Heiss
  AMXSY-GI
    Mr. L. DeLattre

Commander, USATECOM
  ATTN: AMSTE-SI-F

Commander, CRDEC, AMCCOM
  ATTN: SMCCR-RSP-A
    Mr. M. Miller
    Mr. J. Huerta

Director, USAHEL
  ATTN: SLCHE-IS
    Mr. B. Corona
    Mr. P. Ellis

Director, USACSTA
  ATTN: STECS-AS-LA
    Mr. G. Niewenhous

INTENTIONALLY LEFT BLANK.

USER EVALUATION SHEET/CHANGE OF ADDRESS

This Laboratory undertakes a continuing effort to improve the quality of the reports it publishes. Your comments/answers to the items/questions below will aid us in our efforts.

1. BRL Report Number BRL-MR-3810 Date of Report JAN 90

2. Date Report Received ______________________

3. Does this report satisfy a need? (Comment on purpose, related project, or other area of interest for which the report will be used.) ______________________

____

____

4. How specifically, is the report being used? (Information source, design data, procedure, source of ideas, etc.) ______________________

____

____

5. Has the information in this report led to any quantitative savings as far as man-hours or dollars saved, operating costs avoided or efficiencies achieved, etc? If so, please elaborate. ______________________

____

____

6. General Comments. What do you think should be changed to improve future reports? (Indicate changes to organization, technical content, format, etc.)

____

____

____

CURRENT ADDRESS

____
Name

____
Organization

____
Address

____
City, State, Zip

7. If indicating a Change of Address or Address Correction, please provide the New or Correct Address in Block 6 above and the Old or Incorrect address below.

OLD ADDRESS

____
Name

____
Organization

____
Address

____
City, State, Zip

(Remove this sheet, fold as indicated, staple or tape closed, and mail.)

FOLD HERE

Director
U.S. Army Ballistic Research Laboratory
ATTN: SLCBR-DD-T
Aberdeen Proving Ground, MD 21005-5066

OFFICIAL BUSINESS

NO POSTAGE
NECESSARY
IF MAILED
IN THE
UNITED STATES

BUSINESS REPLY MAIL
FIRST CLASS PERMIT NO 12062 WASHINGTON,DC

POSTAGE WILL BE PAID BY DEPARTMENT OF THE ARMY

Director
U.S. Army Ballistic Research Laboratory
ATTN: SLCBR-DD-T
Aberdeen Proving Ground, MD 21005-9989

FOLD HERE